ERDC/GSL TR-01-16

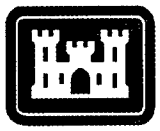

US Army Corps
of Engineers®
Engineer Research and
Development Center

Application of Wavelet Analysis to Logistics Test Vehicle Ride Experiment Results

Andrew W. Harrell, Cliff Grey, and William Willoughby

August 2001

Geotechnical and Structures Laboratory

The contents of this report are not to be used for advertising, publication, or promotional purposes. Citation of trade names does not constitute an official endorsement or approval of the use of such commercial products.

The findings of this report are not to be construed as an official Department of the Army position, unless so designated by other authorized documents.

PRINTED ON RECYCLED PAPER

ERDC/GSL TR-01-16
August 2001

Application of Wavelet Analysis to Logistics Test Vehicle Ride Experiment Results

by Andrew W. Harrell, Cliff Grey, William Willoughby

Geotechnical and Structures Laboratory
U.S. Army Engineer Research and Development Center
3909 Halls Ferry Road
Vicksburg, MS 39180-6199

Final report

Approved for public release; distribution is unlimited

Prepared for U.S. Army Corps of Engineers
Washington, DC 20314-1000

Contents

List of Figures

Preface

Members of the staff of the Geotechnical and Structures Laboratory (GSL), U.S. Army Engineer Research and Development Center (ERDC), Vicksburg, MS, conducted this study during 1999 to 2001. This study was sponsored by Headquarters, Department of the Army, and funding was provided under the AT40 6.2 Research Program, "Lines of Communication, Repair of Roadways," a Science and Technology Objective (STO IV.EN.1998.03).

This study was conducted under the general supervision of Dr. David Horner, Chief, Mobility Systems Branch (MSB), GSL.

The main part of this report and most of the sections on wavelets were written by Dr. Andrew Harrell, MSB, GSL. Mr. Cliff Grey, MSB, conducted the tests in the Logistics Test Vehicle (LTV), processed the data from test instrumentation , and computed some of the wavelet transforms. Dr. John Peters, Soils Research Center, GSL, contributed some of the material on transforms. Dr. William Willoughby, MSB, reviewed the report and added text to improve the clarity of its exposition.

At the time of publication of this report, Dr. James R. Houston was Director of ERDC, and COL John W. Morris III, EN, was Commander and Executive Director.

Conversion Factors, Non-SI to SI Units of Measurement

Non-SI units of measurement used in this report can be converted to SI (metric) units as follows:

Multiply	By	To Obtain
feet	0.3048	meters
inches	2.54	centimeters
miles (U.S. statute)	1.609	kilometers
pounds (force)	4.44822	newtons
pounds (force) per square inch	6.894757	kilopascals
pounds (mass) per cubic foot	16.011846	kilograms per cubic meter
square inches	6.4516	square centimeters
tons	907.184	kilograms

1 Introduction

Background

There are many factors used to determine vehicle trafficability. Some factors, such as soil strength, may even require field measurement or be inferred based on climatic conditions. The NATO Reference Mobility Model (NRMM) developed at the U.S. Army Engineer Research and Development Center (ERDC), Geotechnical and Structures Laboratory (GSL), Vicksburg site, uses the data from over 100 factors that describe a vehicle off-road terrain unit, road unit, or linear feature to predict potential maximum safe vehicular speeds. These factors include surface composition, geometry, vegetation, and linear geometry (Turnage and Smith 1983, Harrell 1989). In order to characterize tactical logistics situations, certain U.S. Army Training and Doctrine Command (TRADOC) operational scenario categories are used with NRMM, such as tactical high (e.g. > 30 kph) or tactical low (< 30 kph) to predict vehicular speeds. Such analyses have been used previously by the ERDC, TRADOC, and the acquisition community (U.S. Army Tank-automotive and Armaments Command (TACOM)) to evaluate the performance of vehicles in given scenarios. Some of the goals of the AT40 6.2 Research Program, "Lines of Communication, Repair of Roadways" are to: (a) develop methodologies and analytic software for determining appropriate convoy speeds, tire pressure, and load capacities on roadway components, and (b) develop methodology to calculate throughput as a function of visibiility and weather conditions. One of the critical parameters that governs speed predictions for a given vehicle is its ride response over areas of terrain and road surface roughness. During force projection operations into underdeveloped or undeveloped countries with poor transportation networks, logistics throughput and maneuver operations will be greatly affected by speed performance and driver ride conditions, especially as roads deteriorate with traffic and changing weather conditions. Thus, given a tactical situation, it is important to develop a means of understanding how to rapidly assess the influence of deteriorating road surface conditions on ride response of vehicles that are used by the force and evaluate this effect in the tactical planning process.

Purpose

The purpose of this study was to develop and recommend a methodology for evaluating tactical support road situations which will assist in determining appropriate convoy speeds, evaluate the use of bypass routes around lost critical nodes in the infrastructure, and allow the computation of road load capacities for determining the logistics vehicle requirements for various tactical scenarios. Thus, the impacts on throughput and maneuver can be evaluated in quantifiable terms.

Scope

Sixteen representative field experiments with a prototype Logistics Support Vehicle (LSV) were conducted at two local test sites, Mound, LA, and LeTourneau, MS. At the Mound site, the test vehicle's accelerometers were calibrated, and two sections of road, one asphalt and one gravel, were used to evaluate the technology under development. At the LeTourneau site, four rock-covered ride courses were used to collect accelerometer and ride meter data over courses with known surface roughness. This report is part of a series of technical reports planned to develop and describe the methodology for using the LSV. The first report described the full characterization of the vehicle dynamic response of the LSV, and this report will describe the methodology developed for using the LSV to assess the impact of road surface conditions in the supply network on logistics throughput. In this report, an innovative methodology using wavelet transforms is developed. These are used to characterize the vehicle's vibrational response to ride conditions while traversing nondeformable areas of known surface roughness. Because the mathematical background necessary to understand the application of wavelets to vehicle vibrational response is relatively new, a short review of wavelet mathematics is also included in this report. Historically, the ERDC has detrended rod and level elevation measurements. Instead of using ride performance of a known vehicle to determine surface roughness, the root mean squared statistic has been used to characterize surface roughness from the detrended elevation values. The development of wavelet technology as an alternative means to characterize the surface roughness of the ride courses through use of the LSV in a similar manner is also described.

2 Test Vehicle, Experiments Conducted, and Data Collected

Logistics Support Vehicle (LSV)

The Logistics Support Vehicle is a militarized research version of the ¾-ton Chevrolet Suburban 4×4. Similar vehicles were purchased by the military under the Commercial Utility Cargo Vehicle program for general and administrative use by ERDC-Vicksburg personnel to measure accelerations at each wheel and the driver's position, in a research effort to determine the effects of deteriorating road surface conditions on vehicle response. Alternatively, the results could be used to estimate road surface deterioration and road life as a function of the traffic speeds, wheeled tire pressure, etc. These data are required for the planning of convoyed military vehicles operating on roads or trails. Long-term research could lead to procedures for characterizing road surface changes on the known response of a specific vehicle used as a calibrated surrogate.

The LSV is a four-wheel drive, diesel-powered, 4×4 carry-all weighing 1,635 lb at the right front, 1,570 lb at the right rear, 1,740 lb at the left front, and 1,685 lb at the left rear, for a total gross vehicle weight of 6,630 lb. The vehicle instrumentation consists of seven accelerometers located on the vehicle and labeled as follows: Ch1 = Front Left Axle, Ch2 = Front Left Frame, Ch3 = Rear Left Axle, Ch4 = Rear Left Frame, Ch5 = Front Right Axle, Ch6 = Front Right Frame, Ch7 = Under the Driver's Seat.

Field Experiment

During March through April 2000, tests were conducted at two sites in the Vicksburg area: Mound, LA, and LeTourneau, MS. The road sections at Mound, one asphalt and one gravel, and four standard test courses at LeTourneau were used for these tests.

a. Mound, LA.

(1) Asphalt road to airport.

(2) Bridge detour road, gravel.

b. LeTourneau, MS.

(1) Ride Test Course 1, rms[1] = 0.77.

(2) Ride Test Course 3, rms = 0.50 (gravel road).

(3) Ride Test Course 4, rms = 1.16.

(4) Ride Test Course 6, rms = 1.81.

Mound, LA

At Mound, the vehicle was operated at a constant speed of 30 mph over the asphalt road and 12 mph over the gravel road, while vibrational data were collected at each accelerated location. These data, along with baseline drop tests conducted with the LSV at ERDC, Vicksburg, to be reported in another report of this series, will be used for three research purposes: (1) characterize the dynamic response of the LSV such that it could be used as a tool for rapidly identifying surface roughness (rms)[1] after being driven over a course or road section, (2) develop criteria for use in predicting the ride performance of a new or concept vehicle as a function of known vehicle parameters related to LSV, and (3) use the LSV baseline response with periodically collected data of a known section of road to estimate the failure rates of road surfaces as a function of traffic type and traffic intensity. These research objectives are being accomplished under the AT40 6.2 Research Program, "Lines of Communication, Repair of Roadways," which is a Science and Technology Objective (STO IV.EN.1998.03)

LeTourneau, MS

At LeTourneau, the vehicle was operated at a variety of constant speeds while traversing ride courses 1, 3, 4, and 6. Sufficient tests were conducted to define the 6-watt absorbed power (ΔP_{vt}) ride course. These data were necessary to characterize the baseline ride dynamics of the LSV over curve of known surface roughness (rms). Results of these tests are shown in Table 1.

---

[1] Root mean squared (rms) = $\sqrt{\sum_i (x_i - x_{i+1})^2}$ where x_I is the measured profile elevation in inches.

Data Collected

For these dynamics response tests with the LSV, eight accelerometers were used. Each was mounted/bonded to a metal mounting block of aluminum and secured to the vehicle at the desired location. These accelerometers are direct current (DC) servo-type (piezo-resistive), which provide excellent stability, high signal-to-noise ratio, and a flat frequency response in the band region. The typical output sensitivity is 5 to 10 mV/g, depending on the selected g range. They provide a frequency response two orders of magnitude higher than typical vehicular acceleration frequency levels and are normally 5- or 10-g range devices. The 10-g accelerometers are mounted on the frame with one mounted on the floor beneath or directly behind the driver's seat of the LSV.

3 Background to Wavelet Analysis

What are Transforms?

Transforms are the result of transforming a function of one independent variable to that of another. A common example of a transform of $f(t)$ is the cosine transform

$$f(t) = \sum_{k=0}^{\infty} A_k \cos(2\pi \frac{kt}{T}) \tag{1}$$

or

$$f(t) = \sum_{k=0}^{\infty} A_k \cos(2\pi\omega_k t) \tag{2}$$

where $\omega_i = k/T$ is the frequency. The cosine transform of $f(t)$ is literally the coefficients in the series $A_k = A(\omega_i)$ which are given by

$$A_k = \frac{2}{T} \int_0^T f(t)\cos(2\pi\omega_k t)dt \tag{3}$$

Thus, the function in the *time domain* is transformed to a function in *frequency domain*. The cosine transform is an example of a more general class of *linear* transforms referred to as *Fourier* transforms. Note that the transform is a *linear* combination of the sequence of cosine functions, (a property of the transform), and the constants A_k (a property of the data). The cosine functions are referred to as the *basis* functions or *kernel* of the transform. Other choices of basis functions give different transforms having different properties.

Consider a function as a list, or time record, of N numbers that is a discrete sampling of a continuous function in time, $f(t)$. The readings are equally spaced over a total time of $T = N\Delta t$ such that the position, k, in the list corresponds to a

time equal to $k\,\Delta t$. In the discrete transform, the list of N samples in time is transformed to a list of N numbers, each corresponding to a discrete frequency. Each record can be computed from the summation

$$f_n = \sum_{k=0}^{N} A_k \cos(2\pi\omega_k n\Delta t) \tag{4}$$

For the general discrete Fourier transforms, the basis functions consist of both sines and cosines,

$$f_n = \sum_{k=0}^{N} [A_k \cos(2\pi\omega_k n\Delta t) + B_k \sin(2\pi\omega_k n\Delta t)] \tag{5}$$

which is generally written in *complex form* as

$$f_n = \sum_{k=-N/2}^{k=N/2} F_k \exp(i\pi\omega_k n\Delta t). \tag{6}$$

The algorithm for computing this transform efficiently is referred to as the *Fast Fourier Transform* (FFT).

Why Use Transforms?

The transformed data carry the same information as the original record, whereby given the transform the original data can be retrieved. However, the transformed data are sometimes a more useful *representation*. For example, the resonant frequency of the vehicle and the roughness of the road might dominate the record of a road test. The time-domain record might not show the superposed effects, whereas the two effects would be obvious in the frequency domain. *Filtering* the effect of roughness from the record amounts to removing those data from the frequency domain and transforming the result back to the time domain. *Data compression* techniques make use of the dominance of particular frequencies in a record. Compression is achieved by storing or transmitting only the F_k that are significant; decompression then is the transforming back to the time domain to obtain an approximate record that is now missing the (presumably) irrelevant data. Unfortunately, not all transforms are equally efficient. For example, a record that contains only one nonzero value (a spike) is most efficiently represented in the original time domain. In the frequency domain representation of a spike, each element of the Fourier transform has the same value.

What are Wavelets?

Wavelets are mathematical families of functional atoms or functional components. They can be generated from a single function, Ψ, by dilations and

translations in the form: $\psi_{a,b} = |a|^{1/2}\psi((t-b)/a)$; where the parameters a and b are often restricted to a discrete set. In this form they provide a way to decompose an arbitrary function similar to the way sines and cosines are used in the mathematical theory of Fourier analysis. Wavelet Transforms are defined and used in wavelet methods to analyze signals in a way analogous to Fourier Transforms:

For a and b, arbitrary positive or negative real numbers, the discrete wavelet transform (DWT) is

$$(Tf)_m = \langle \psi_{m,n}, f \rangle = |a_0|^{-m/2} \int dt * \psi(a_0^{-m} t - nb_0) * f(t) \qquad (7)$$

where $a = a_0^{\,m} \qquad b = nb_0 a_0^{\,m}$

These methods provide an improved way to analyze and represent functions in the spatial form, the representations of which are changing with time. The book by Krantz (1999) gives a good overview of some of the mathematical topics in the theory of real analysis and functional analysis, which played a part in their invention and development.

The uses of wavelets are varied. Fournier (1995) contains an introduction to their use in computer graphics and image compression, and Charles Chu (1997) explains their uses to improve the functional representation by interpolation of splines of data for numerical partial differential equations. The papers by Newland and Butler (1999a,b) use wavelets for the study of centrifuge experiments related to earthquake engineering. The reference by Torrence and Compo (1998) provides data on using them to prove the statistical significance of El Nino related sea surface temperatures.

And, corresponding to their different uses, there are many different types of wavelets: continuous wavelets (Meyer and Ryan 1993), discrete wavelets (Chu 1997), orthogonal wavelets, biorthogonal and compact wavelets (Daubechies 1992). The Daubechies scaling function, wavelet function, and filter coefficients are shown in Figure 1. The definitions of the scaling function and wavelet function are based on the mathematical algorithm used to compute the wavelet decomposition by Chu 1997. The wavelet filter coefficients are the multipliers used in the wavelet transform to extract the high- and low-frequency components of the signal. Chu 1997 has a good reference to help understand how wavelet function, scaling function and filter coefficients work together to decompose, reconstruct, and approximate the signal.

The wavelet decomposition process is initiated by first separating a signal into two parts, an approximation part A1 and a detailed part D1. This is accomplished by using the coefficients of a high- and low-pass filter, which multiply the wavelet and scaling function. In the next level (step), the approximation A1 is itself separated into two parts, A2 and D2. This process decomposition is repeated until the final level of wavelet approximation is reached.

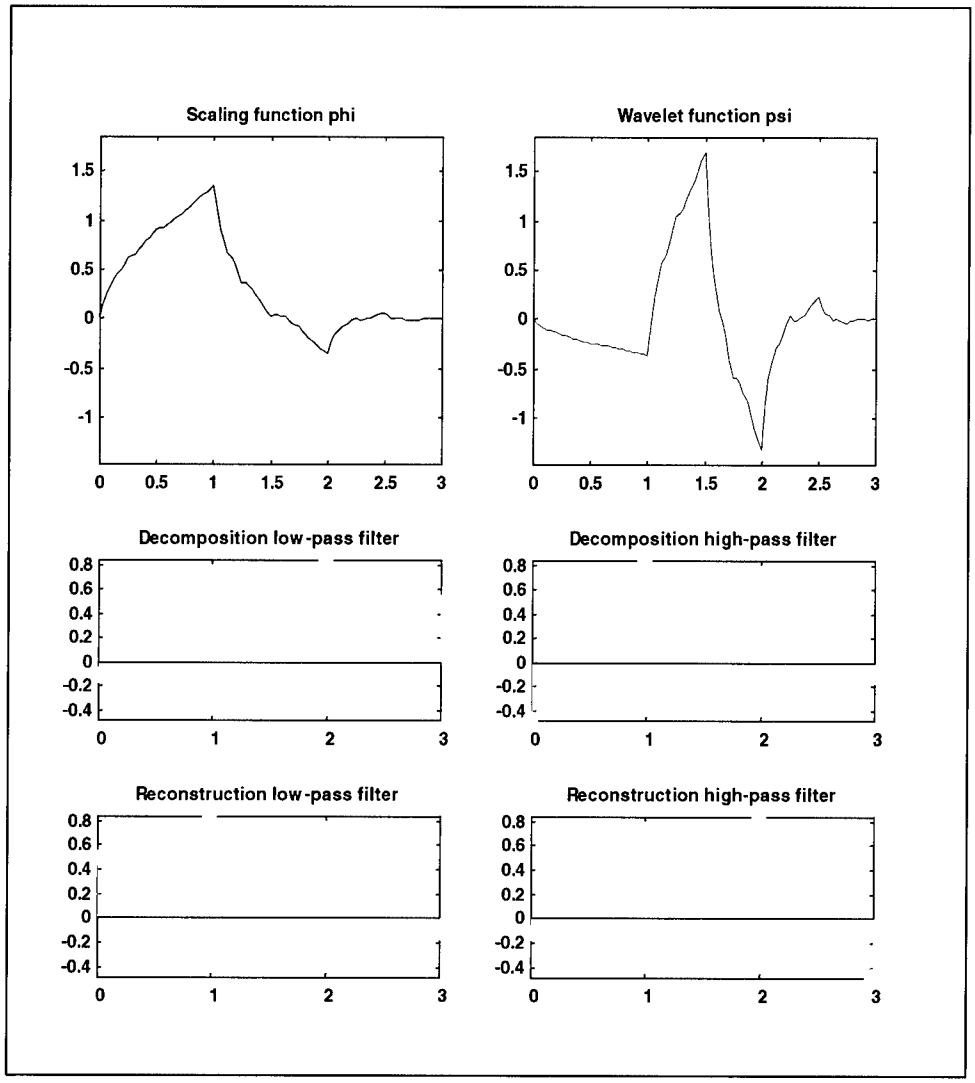

Figure 1. Example of wavelets

This report will primarily consider Daubechies (1992) wavelets and Meyer and Ryan (1993) wavelets as defined in the MATLAB wavelet toolbox (Misiti et al. 1996), and harmonic wavelets as defined by Newland (1993). The harmonic wavelets were picked for their usefulness in analyzing time series data from vibrational studies such as those reported in the following: "For the purposes of signal analysis, a wavelet is considered to be a bandpass window function that stops at least the zero frequency" (Chu 1997).

Wavelet packets are a generalization of wavelets, which use two high and two low bandpass filters instead of one each (Misiti et al. 1996, Mallat 1998, Meyer and Ryan 1993, Chu 1997). Wavelet packets are more often used for one-dimensional (1-D) signal analysis (as opposed to two-dimensional (2-D) image compression), because they do a better job of representing the time-dependence of the signal. They use a family of two sets of orthogonal bases to decompose the signal, instead of one. An optimal base inside of the family can be chosen that

minimizes the sum of squares of residuals of the signal values and the wavelet approximation. This optimal wavelet base is often represented in terms of a particular wavelet decomposition tree. The wavelet packet decomposition process begins similarly to the wavelet decomposition process. First, the signal is separated into two parts, an approximation part A1 and a detailed part D1. This is accomplished by the coefficients of high- and low-pass filters, which multiply the wavelet and scaling function. Now, in contrast to the wavelet decomposition process, in the next level (step) of the packet decomposition, the approximation A1 is separated into two parts, A21 and A22, and the detailed D1 is separated into two parts, D21 and D22. This is a composition, as mentioned above, by using two orthogonal bases for the decomposition. One base corresponds to the scaled and translated time/frequency atomic terms generated by the "mother" wavelet function. The other base corresponds to the scaled and translated time/frequency atomic terms of a dual "father" wavelet function. The process is repeated until the final level of wavelet approximation is reached.

The 2-D plot of the square of the signal approximation in space and in time is called a Heisenberg box (Mallat 1998). These plots can be examined to determine the best way to subdivide the spatial and temporal axes to compute the wavelet bases.

Figure 2 shows a wavelet decomposition tree and the Heisenberg box for the decomposition of a power spectral density function. The x-axis of the signal (figure in the upper right box) is frequency and the y-axis is the square of the amplitude of the Fourier transform of the starting signal. The x-axis of the box (figure in box at lower right) is time and the y-axis is frequency. The number of boxes on the vertical y-axis corresponds to the number of frequency decomposition nodes on the lowest level in the wavelet decomposition tree.

Reasons for the Use of Wavelets in Vibrational Analysis Studies

The tutorial by Polikar (1999) gives a beginner's introduction for engineers on the use of wavelets for signal analysis. And, the more advanced reference by Daubechies (1992) contains most of the pertinent basic theorems in mathematical analysis, which are necessary to justify the use of wavelets to analyze time series data. Fourier transformations separate different parts of the data, which correspond to its different cyclic components. They allow an experimenter to examine the behavior of a system in both the spatial and frequency domains. In signal analysis, a series of related data observations taken over a period of time is called a time series. If the statistical parameters that characterize different parts of the series of data vary with respect to time, the time series is said to be nonstationary. (Otherwise, it is said to be stationary.)

There are several reasons why it is advantageous to use Wavelet transforms instead of the more familiar Fourier Transform to analyze time series:

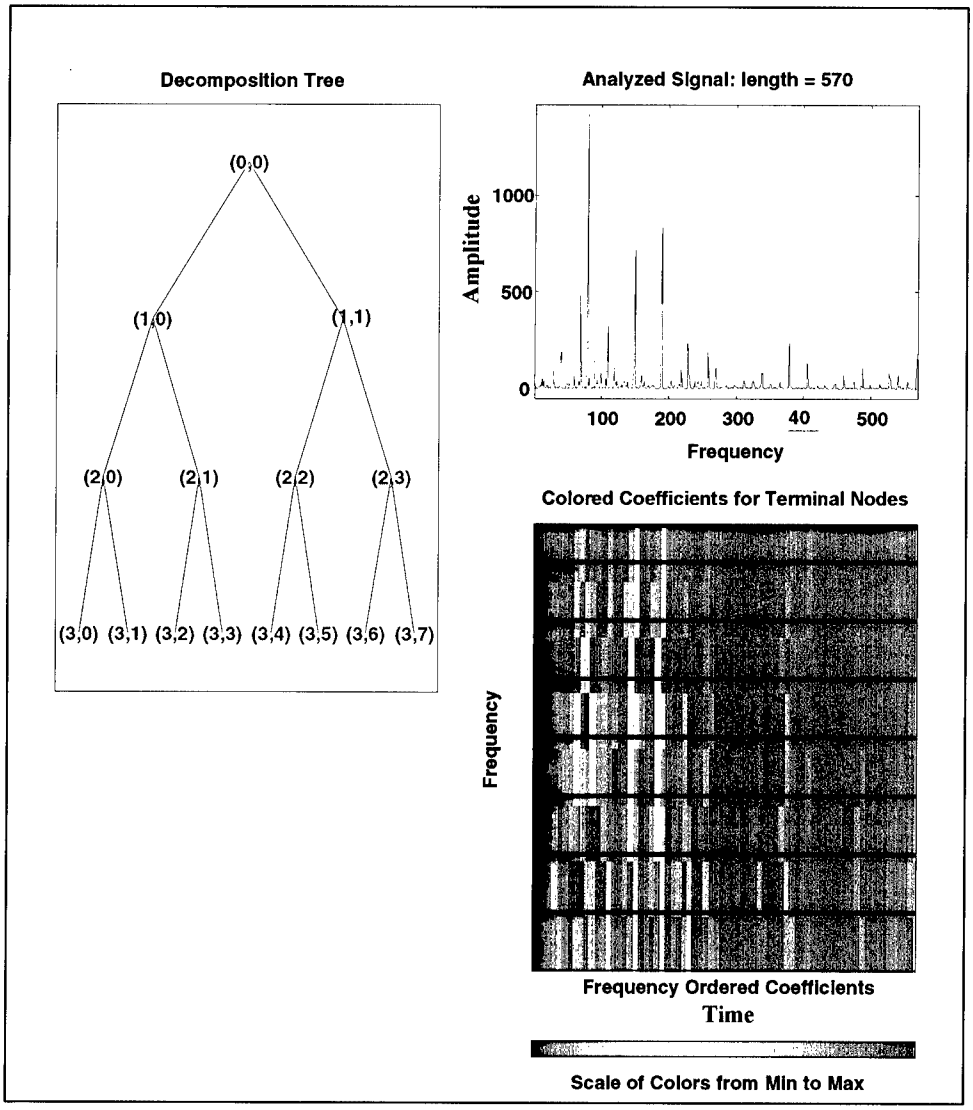

Figure 2. Example of wavelet decomposition

"A disadvantage of Fourier analysis is that the frequency information can only be extracted for the complete duration of a signal. Since the integral in the Fourier transform extends over all time, the information it provides arises from an average over the whole length of the signal. If, at some point in the lifetime of the signal, there is a local oscillation representing a particular feature, this will contribute to the calculated Fourier transform, but its location on the time axis will be lost...By breaking the signal into shorter and shorter time segments, using windowing functions and dilation equations, wavelets analyze and extract this local information...Fourier analysis fails to capture the non-stationary aspects of the time series, but, the wavelet approach allows these factors to be characterized." (Newland, 1993 (p. 294)).

Harmonic Wavelets

Harmonic wavelets are certain combinations of Gabor wavelets introduced in the book by Newland (1993). Harmonic wavelets are Gabor wavelets; thus, they are wavelet packets as we defined them previously. Dennis Gabor introduced Gabor wavelets in 1946 in a study of speech analysis and reconstruction. They facilitate the representation of time signals as a superposition of elementary wavelets. If the signal is expected to have a certain temporal structure as well as certain emitted frequencies, it is necessary to analyze the signal's properties both with respect to its frequencies and the time when they were emitted. As explained by Walker (1999) and Meyer and Ryan (1993), a Gabor wavelet of width parameter w and frequency parameter v has a wavelet function.

$$\psi(x) = w^{-1/2} * e(-\pi(x/w)^2) * e(i * 2\pi * v * (x/w)) \tag{8}$$

The independent variable in this equation is a real variable. Harmonic wavelet packets have a wavelet function of a complex variable

$$\psi(\mathrm{x}) = (\mathrm{e}(-4\pi * \mathrm{x}) - \mathrm{e}(\mathrm{i} * 2\pi * \mathrm{x}))/(\mathrm{i} * 2\pi \mathrm{x}) \tag{9}$$

So, they are a combination of two complex Gabor wavelets of frequency parameters 4 and 2 and each with width parameter 1. A disadvantage of using this wavelet is that it decays on the x-axis only proportional to 1/x. Thus, the theorems in Meyer (1993) and Daubechies (1992) concerning r-regular wavelets, where $r > 1$, do not apply. This wavelet function does, however, generate an orthogonal basis, which can be used for multiresolution analysis.[1] And, in many cases, its simple analytical formula is an advantage. Also, since the wavelet function is complex, only one-half as many coefficients need to be computed to determine its value at each translation and dilation index.

Figure 3 shows a wavelet function and the windowing transforms for the wavelet and scaling functions for a set of harmonic wavelets, which will be used in this report.

If regularity and vanishing moments of the approximation functions are important, Meyer wavelets can be used. These wavelets are analytic, symmetric, with a compactly supported[2] Fourier transform, and their size decays faster than any polynomial. They are shown in Figure 4. The paper by Abry, Goncalves, and Flondrin (1995) discusses the advantages of using wavelets with r vanishing moments to perform power spectral estimation. The book by Kay (1988) is a good introduction to the general area of power spectral estimation and the problems involved in constructing good statistical sampling algorithms for it.

---

[1] These theorems guarantee that the square norm of Fourier transform of wavelet function is infinitely differentiable, and that the first r moments of the wavelets coefficients are zero. This makes them desirable to use as approximations and interpolations.

[2] A function is compactly supported if the part of its domain of definition where it is nonzero contains all its limit points and is a bounded set with respect to distance.

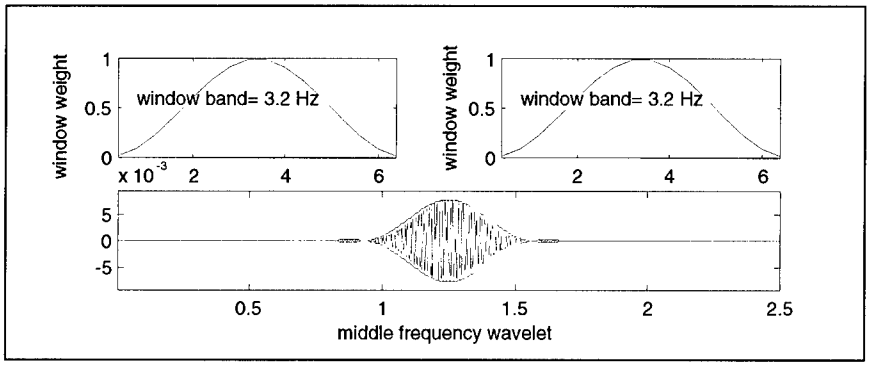

Figure 3. Harmonic wavelets

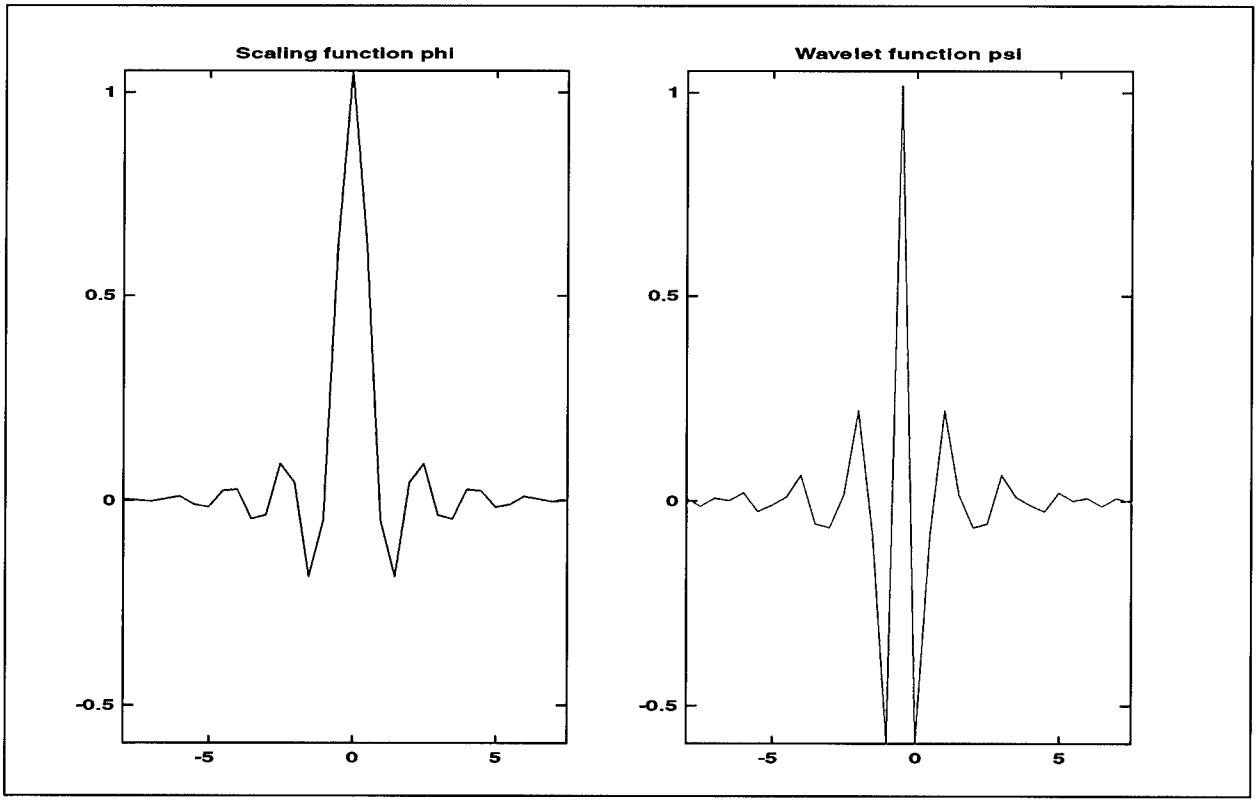

Figure 4. Meyer wavelets

Meyer Wavelets

Yamada and Sasaki 1998 describe the use of Meyer wavelets (Figure 4) for the analysis of atmospheric wind, turbulent fluid, and seismic acceleration data. As mentioned previously, the wavelet function decreases to zero when x increases to infinity faster than any polynomial. This property also holds for the derivatives of this wavelet function. These wavelets are analytic, symmetric, and orthogonal.

4 Wavelet Analysis for the Ride Experiments

General Background

The subject of random vibrations as they relate to the dynamic projection of a vibrating vehicle (mass, stiffness, damping, etc.) and the understanding of the statistical characteristics of the motion generated by operating over on-/off-road terrains will be very important as the Army transforms into the 21st century. Typically, analysis of vehicle motion transforms produces vibration data averaged over sections of roads or trails. Local position of particular features or sections of interest is lost with Fourier analysis. Wavelets are a recent development in signal analysis, which allows decomposition of the signal into a series of other generally orthogonal functions of different lengths and positions with respect to time. Features producing extreme or unusual vibration can be located using the positions of the wavelets into which the signal can be decomposed. In this manner, vehicle vibrational data collected in the time domain may mask the most distinctive information, which is hidden in the frequency content of the signal test. The FFT algorithm produces frequency domain coefficients, which describe the amplitude and phase of the signal's harmonic components. The disadvantages of analyzing only time-domain data or frequency domain FFT data are defeated through use of wavelet analysis, which maintains both time and frequency resolution. The application of this relatively recent technology to the LSV is discussed in this report.

In this study, raw data collected with the LSV on roads at Mound, LA, at 100 samples/sec per channel were stored in units of g.[1] The interactive software package MATLAB, with a wavelet toolbox written by Newland (1993), was used to evaluate the data collected at Mound, LA. Using discrete wave transforms (DWT), transformation plots were created as shown in Figures 5 and 6. In Figure 5, which is a 2-D frequency versus time-color plot, the black-to-red background indicates normal noise levels. While the energy in the raw signal increases, the color changes from the red to a hotter color much like steel changes color as it is heated. Yellow/white indicates higher energy levels. Figure 6 is a 3-D frequency versus time-color plot similar to the previous figure, but it is shown

[1] The acceleration of gravity, 32 ft/sec^2

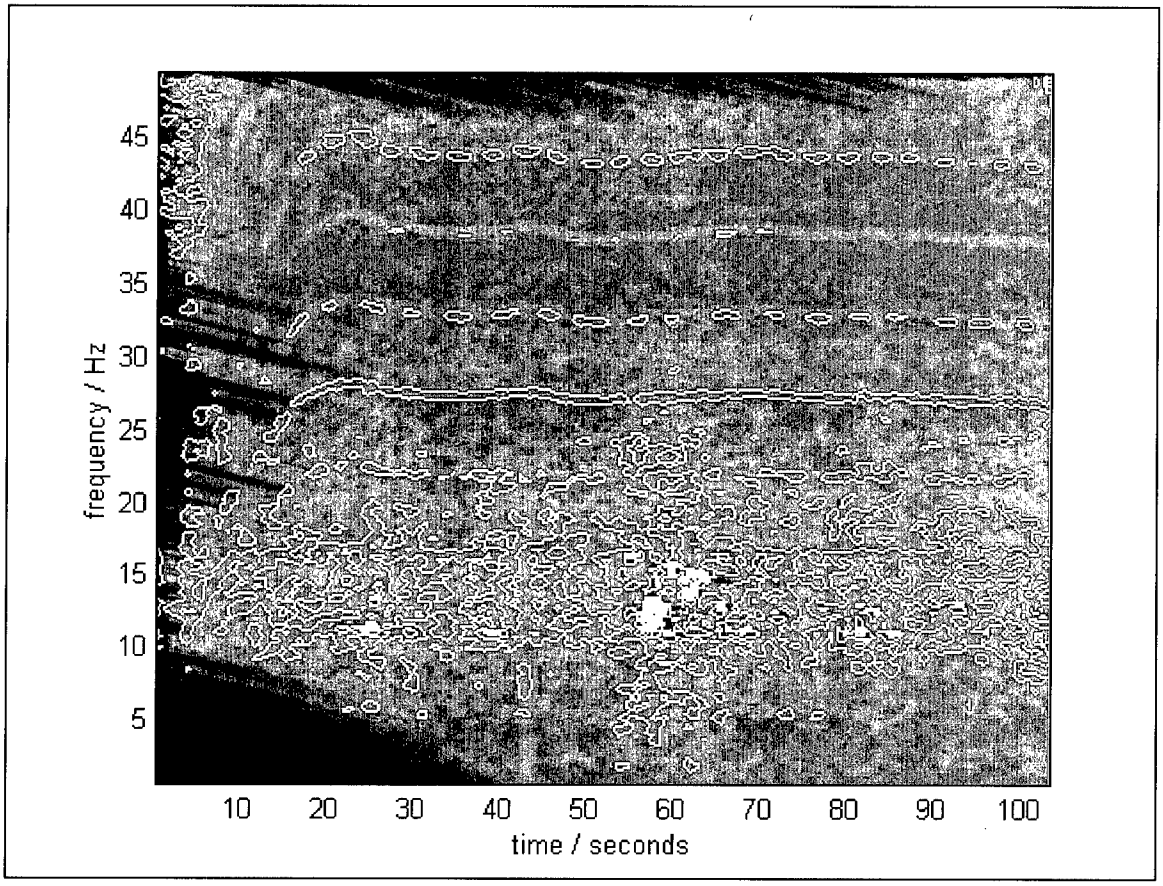

Figure 5. Wavelet power spectrums versus time

from another view angle. The yellow vertical rises above the reddish background indicate rough areas of the paved road.

Similarly, the MATLAB toolbox was used to evaluate the raw data from the gravel road used as a bypass of the bridge. There results are presented in Figures 7 and 8 for the data collected on the left front axle of the LSV. Comparison with the paved road test data clearly indicates the differences in energy levels while riding over the gravel road versus the paved road. Note the difference in the color variations between the two plots.

Mound Test Track Data Results: Wavelet Analysis, 3/17/00

These are the results of data taken Friday, March 17, 2000, at the Mound, LA, test track. These data include the segment of road turning off of Highway 80 down past the airport to the bridge detour. The section of road was paved with asphalt and relatively smooth.

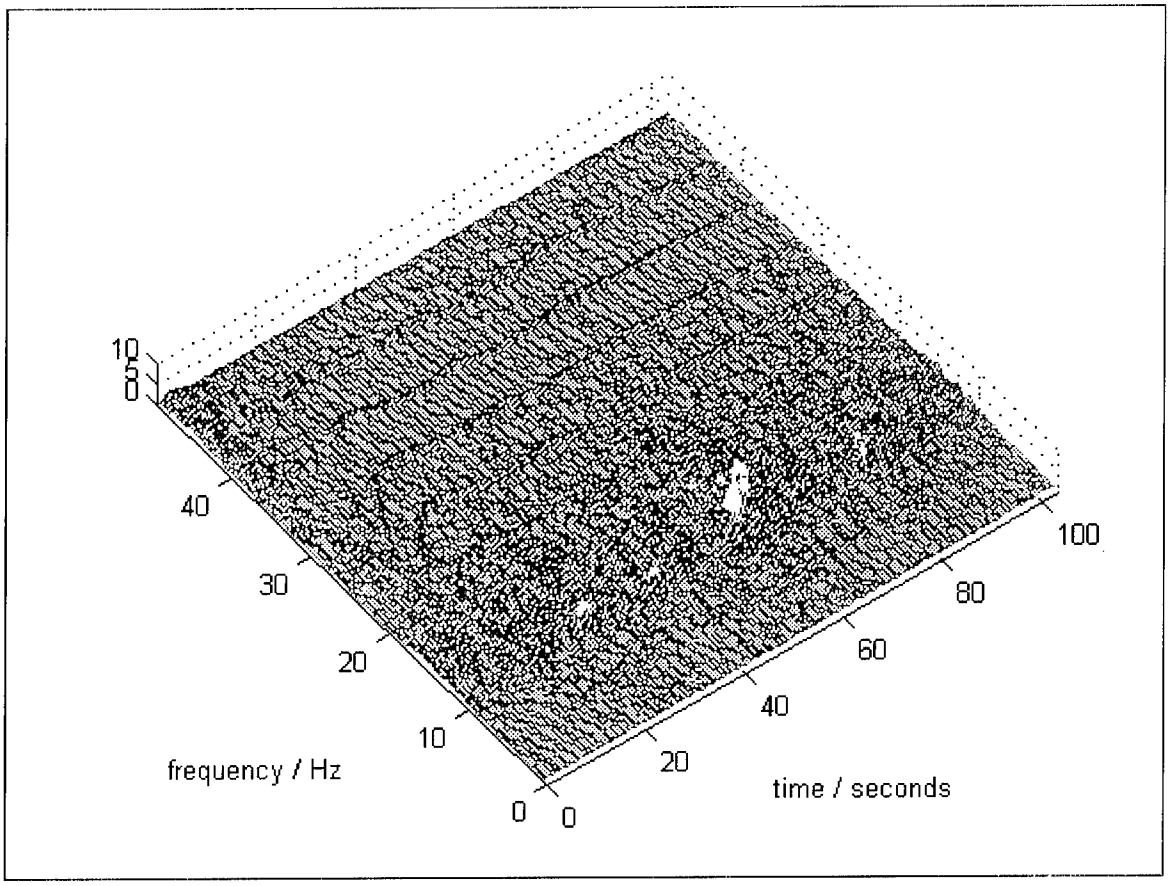

Figure 6. 3-D wavelet power spectrum versus time

There are seven accelerometers located on the vehicle which are labeled as follows: Ch1 = Front Left Axle, Ch2 = Front Left Frame, Ch3 = Rear Left Axle, Ch4 = Rear Left Frame, Ch5 = Front Right Axle, Ch6 = Front Right Frame, Ch7 = Under the Driver's Seat.

All segments of the track were run at a near constant speed of 30 mph with exception of the bridge detour area, which was traversed at approximately 12 mph. All of the accelerometer outputs are in engineering units calibrated to g forces (g's). The following plots are transformations on the raw data using wavelet analysis called DWT.

Beginning with the first channel, front left axle, there are two plots of data associated with this channel. Figure 7 is a 2-D frequency versus time-color plot, and Figure 8 is a 3-D frequency versus time-color plot. It is very much the same as Figure 7 but is shown at a different angle. One can look at this figure and determine rough spots in the road.

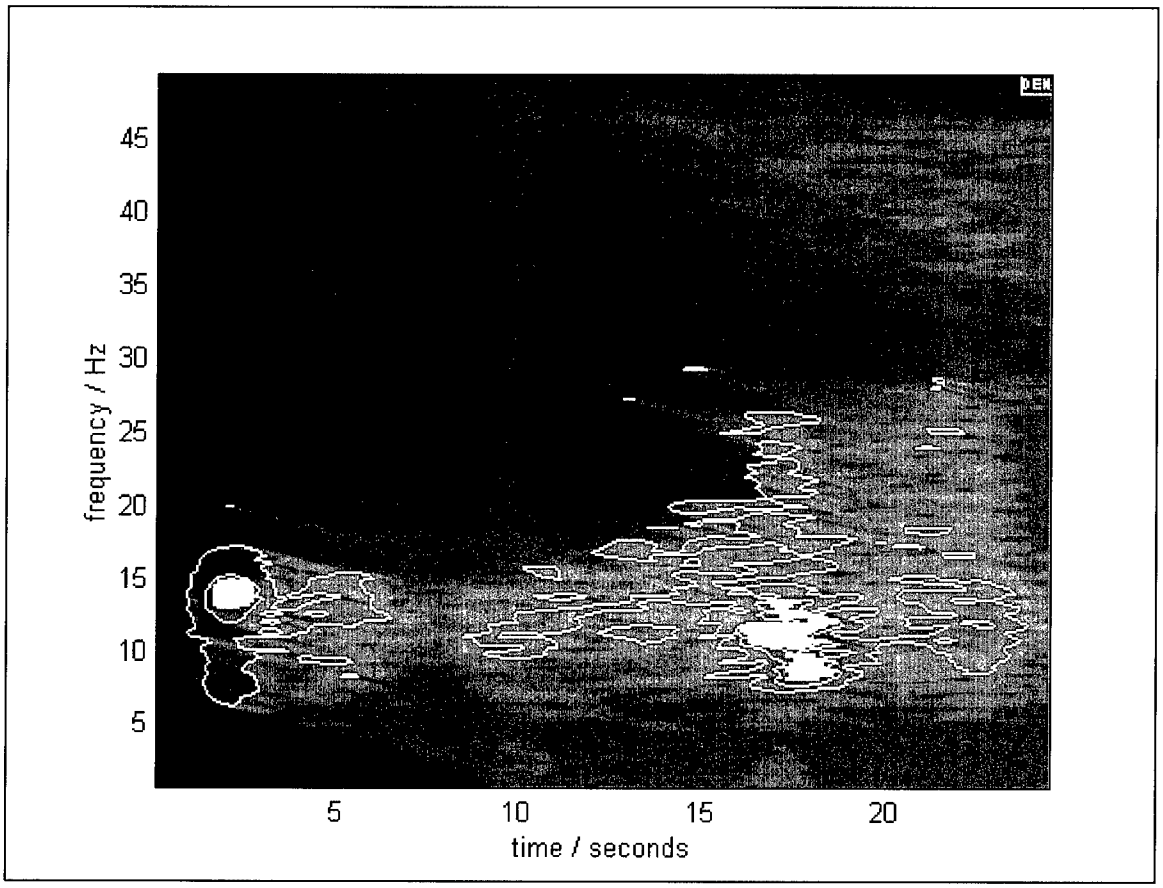

Figure 7. Channel 1, front left axle, 2-D plot

Mound Test Track Data Results: Wavelet Analysis, 3/24/00

Bridge Detour. These are the results of data taken Friday, March 24, 2000, at the Mound, LA, test track. These data include the brief segment around the bridge detour.

There are seven accelerometers located on the vehicle which are labeled as follows: Ch1 = Front Left Axle, Ch2 = Front Left Frame, Ch3 = Rear Left Axle, Ch4 = Rear Left Frame, Ch5 = Front Right Axle, Ch6 = Front Right Frame, Ch7 = Under the Drivers Seat.

This segment of the track was run at a near constant speed of 30 mph with exception occurring at the bridge detour area, which was traversed at approximately 12 mph. All of the accelerometer outputs are in engineering units calibrated to g forces (g's). The following plots are transformations on the raw data using wavelet analysis called DWT (discrete wave transform).

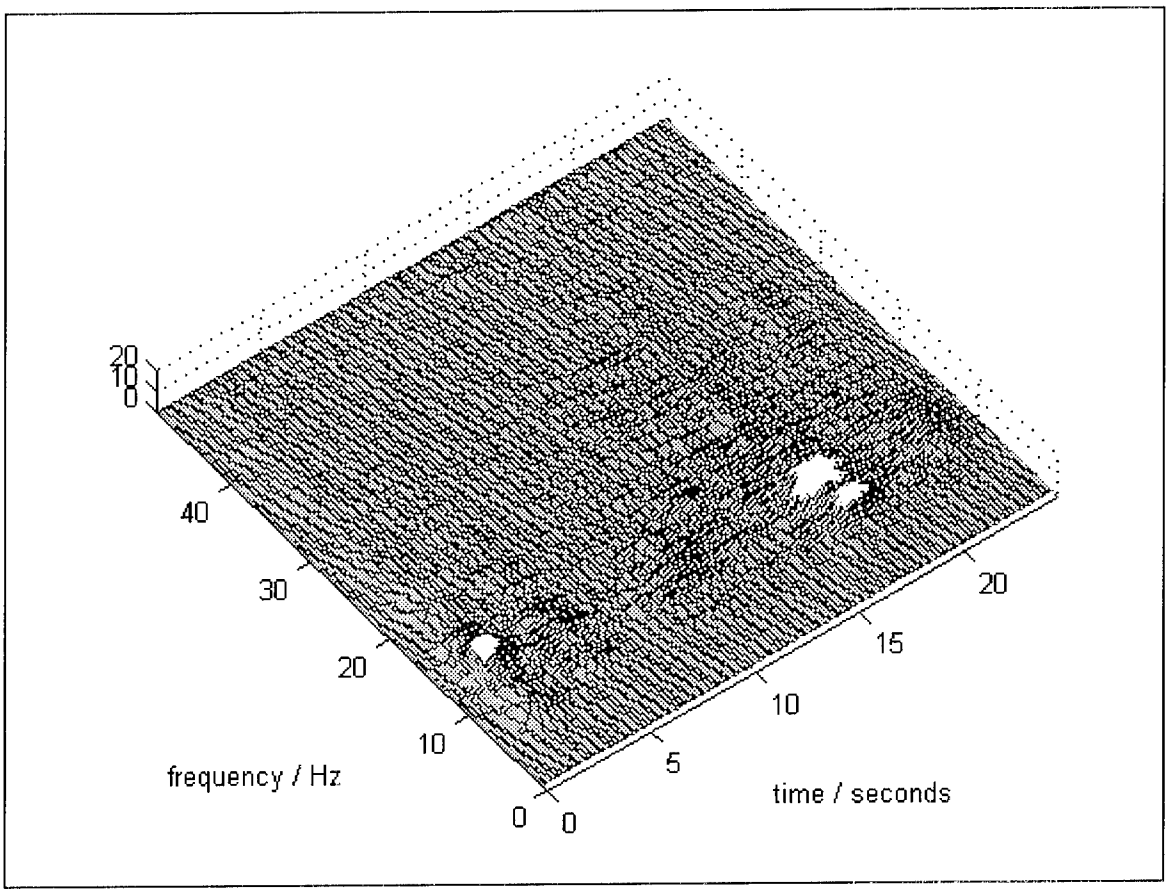

Figure 8. Channel 1, front left axle, 3-D plot

Ride and shock assessment: LeTourneau test track

1 Apr 00 -- Introduction and test description. The objective of this experiment was to correlate historical data collected with the U.S. Army Engineer Waterways Experiment Station (WES) (currently known as ERDC) Ride and Shock Meter and the high-speed data collection system that currently resided on the vehicle. The WES Ride and Shock Meter measures human body response, whereas the VIPER system on the LSV measures road surface conditions by measuring vehicular response. By mounting accelerometers in and around the vehicle in nontraditional locations, this analysis will attempt to narrow the scope of the problem and lead to a viable method for characterizing varying road conditions.

Seventeen data files were collected with the high-speed data acquisition system, and, as a comparison, sixteen test sets were collected to measure absorbed power with the WES Ride and Shock Meter. The WES Ride and Shock Meter measures the absorbed power that is subjected to the driver through means of an accelerometer mounted on the driver's seat just below the groin area. The high-speed system uses seven accelerometers mounted in various locations on the vehicle to measure acceleration. The accelerometer inputs are recorded through a

calibrated amplifier system and the recorded engineering units are in g's. Their locations are as follows:

a. Channel 1 – Front Left Axle.

b. Channel 2 – Front Left Frame.

c. Channel 3 – Rear Left Axle.

d. Channel 4 – Rear Left Frame.

e. Channel 5 – Front Right Axle.

f. Channel 6 – Front Right Frame.

g. Channel 7 – Under the Driver's Seat.

h. Channel 8 – Speed.

Several courses were traversed at different speeds. Namely, Ride Course 1 (north and south at 10, 15, and 20 mph), Ride Course 4 (north and south at 5, 15, and 20 mph), Ride Course 6 (north and south at 10 mph), and the gravel road were traversed north and south at 20 mph.

Table 1 lists the raw data files and their correspondence to the event sequence along with how the files are related as to distance, direction, and speed. The speed at which these lanes were actually run represent a true and steady speed. The slower speeds were easier to maintain than the higher speeds.

Table 1
Experiment Program

File Name & #	Ride Meter #	Ride Course	North / South	0-500/500-0	Speed
Letourne.prn	Na	4	S	0-500	10
Letourne0.prn	Na	4	N	500-0	20
Letourne1.prn	1	1	N	500-0	10
Letourne2.prn	2	1	S	0-500	10
Letourne3.prn	3	1	N	500-0	15
Letourne4.prn	4	1	S	0-500	15
Letourne5.prn	5	1	N	500-0	20
Letourne6.prn	6	1	S	0-500	20
Letourne7.prn	7	4	S	0-500	5
Letourne8.prn	8	4	N	500-0	5
Letourne9.prn	9	4	S	0-500	15
Letourne10.prn	10	4	N	500-0	15
Letourne11.prn	11	4	S	0-500	20
Letourne.12.prn	12	4	N	500-0	20
Letourne13.prn	13	6	N	500-0	10
Letourne14.prn	14	6	S	0-500	10
Letourne.15prn	Na	6	S	0-500	10
Letourne.16prn	15	3 (Road)	N	500-0	20
Letourne.17prn	16	3 (Road)	S	0-500	20

Results from ride meter

The following figures, Figures 9 though 12, are typical plots generated using the WES Ride and Shock Meter. The plots show absorbed power as a function of speed.

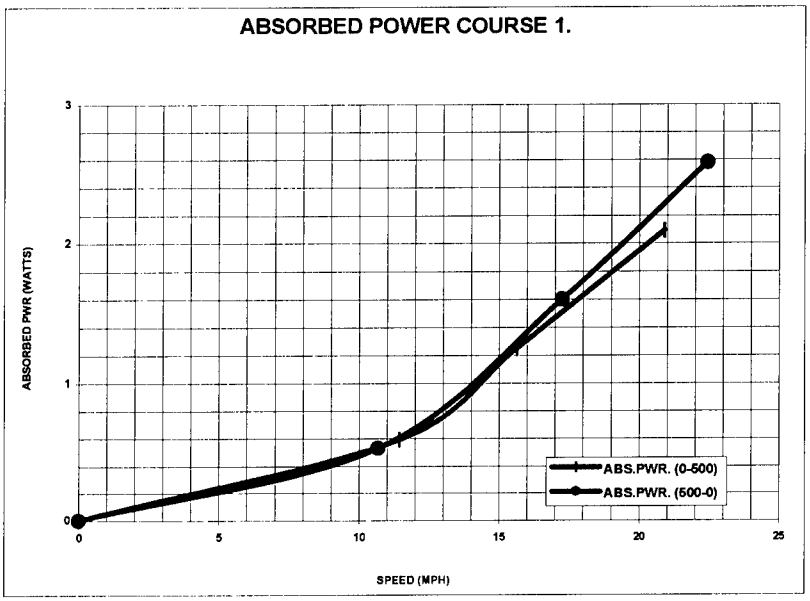

Figure 9. Absorbed power plot for Course 1

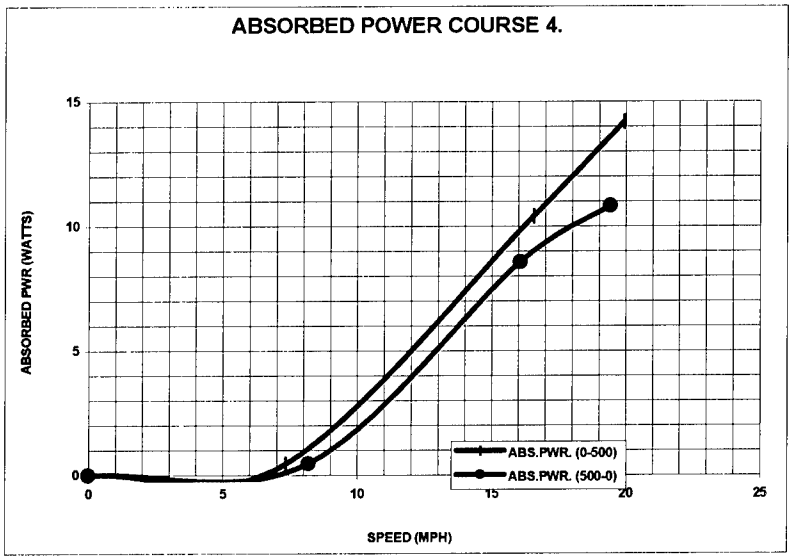

Figure 10. Absorbed power plot for Course 4

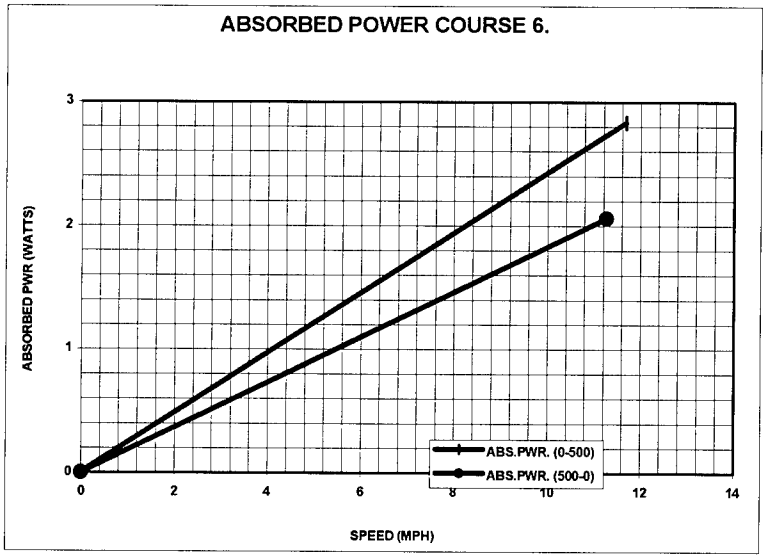

Figure 11. Absorbed power plot for Course 6

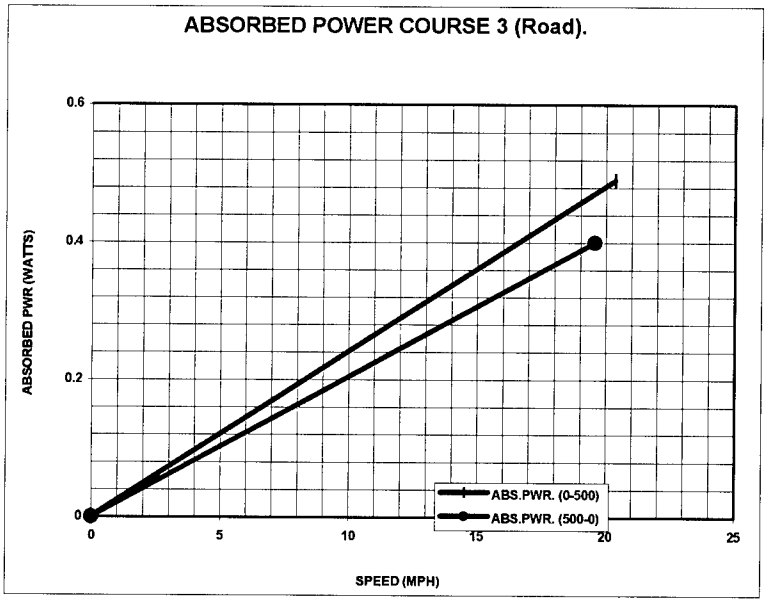

Figure 12. Absorbed power plot for Course 3 (Road)

Wavelet Analysis of the Ride Courses

At the LeTourneau ride test courses, a sufficient number of tests at varying speeds were conducted to determine the 6-watt absorbed power in the vertical direction (ΔP_{rt}) versus surface roughness (rms, in.) relationship for the LSV, using ride courses 1, 3, 4, and 6. Their data are presented in Table 2. The raw

Table 2
Raw Data of Taken with the WES Ride and Shock Meter

Test #	Time	Speed, sec	Watts	Iso Rms	Peak Acc	Pips
1	31.88	10.69	0.53	0.06	0.4	500
2	29.75	11.45	0.59	0.06	0.5	500
3	19.74	17.26	1.6	0.11	0.68	500
4	21.77	15.65	1.25	0.1	0.63	500
5	15.18	22.45	2.58	0.14	0.73	500
6	16.3	20.91	2.09	0.12	0.63	500
7	46.34	7.35	0.44	0.05	0.5	500
8	41.55	8.2	0.46	0.05	0.45	500
9	20.56	16.58	10.4	0.3	1.75	500
10	21.2	16.08	8.57	0.28	1.51	500
11	17.08	19.95	14.18	0.35	1.89	500
12	17.55	19.42	10.82	0.3	1.42	500
13	29.14	11.69	2.83	0.17	0.97	500
14	30.23	11.27	2.06	0.15	0.75	500
15	16.73	20.37	0.49	0.06	0.44	500
16	17.41	19.58	0.4	0.05	0.42	500

frequency data collected for the ride tests were next subjected to wavelet analysis as per the Mound road data. By the process of trail-and-error using the MATLAB Toolbox, those wavelet families which appear to be most applicable are Daubechies (1992) and Meyer and Ryan (1993). The elevation profile analysis of the first portion of the 500-ft LeTourneau Ride Course 1 is shown in Appendix A, Figure A1.

The elevation profile shown in Appendix A is of the left track of LeTourneau Ride Course 1. The rms of this track of the course is 0.92. Figure A2, Appendix A, shows the detrended version of the elevation profile.

The frequency components in the ride course themselves as well as those of the vehicle's response can be subjected to wavelet frequency analysis. The frequency analysis of the first part of the Letourneau Ride Course 1 is shown in Appendix A. The graphs, Figure A1 through A6, Appendix A, show a Daubechies (1992) wavelet analysis of the detrended ride course elevation density. Both the full 300 ft and separately the first 120 ft of the LeTourneau Ride Course 1 (from the data in Figure A2, Appendix A) are analyzed. A Daubechies multilevel decomposition was completed using the second Daubechies wavelet family. The top left graph in Figure A5 is the level 3 approximation to the spectral density. The remaining graphs in Figure A5, display the next three levels of detail in the wavelet analysis. The ratios of the magnitudes of the values on the y-axis of the details versus the approximation indicate that it is hard to characterize the ride course by this type of approximation.[1] This result supports the

[1] Methodology for the wavelet approximations is that in the MATLAB toolbox book by Misiti et al. (1996).

conclusion that the root mean squared value of the course distinguishing the courses is adequate to characterize the courses for experimental analysis of the vibrational response of the vehicle. The wavelet analysis did not show that a significant part of the frequency power spectrum of the course was left in the details of the first three levels of approximation to the signal. Thus, one would expect a Fourier transform or wavelet transform to not be affected by the response of the vehicle's vibrations to this part of the input. And, this supports the notion that the root mean square statistic is adequate to characterize the course for experimental analysis.

Figures 13 and 14 show the results of harmonic wavelet analysis of the LSV's test response to Letourneau Ride Course 1.

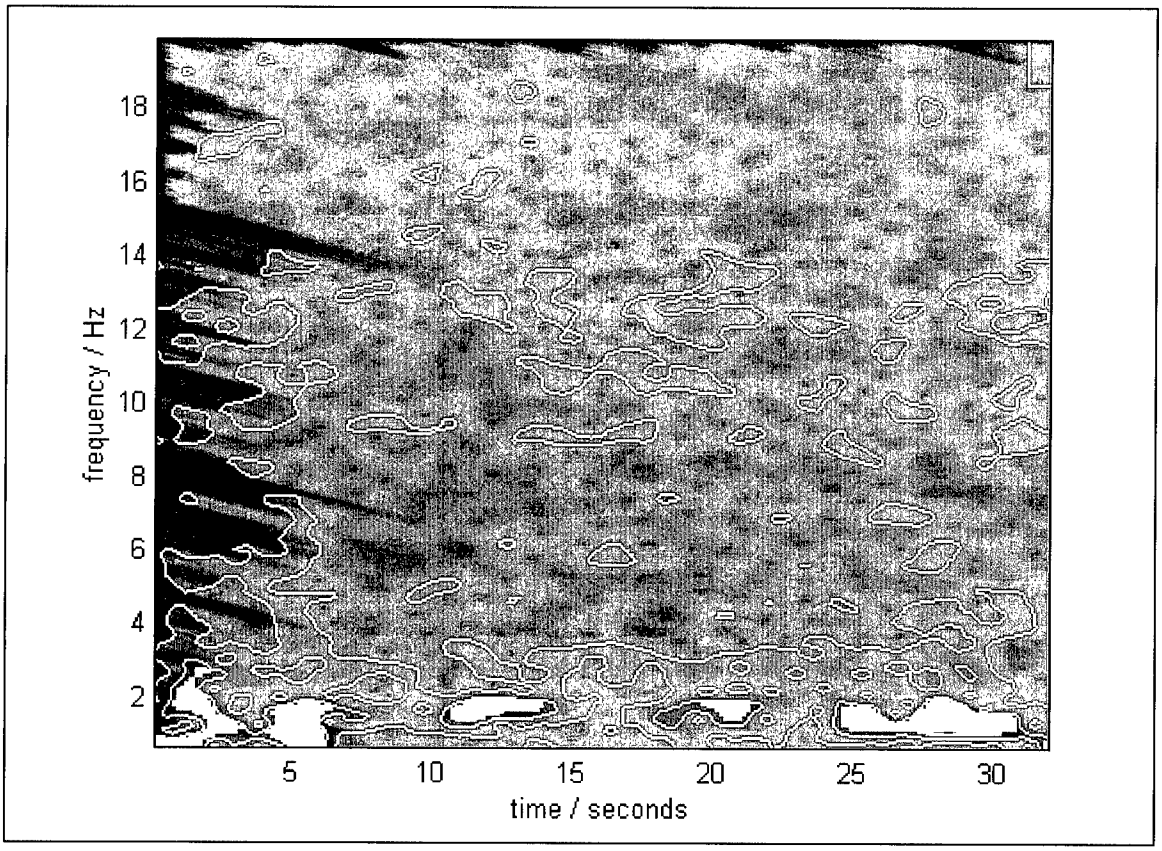

Figure 13. Channel 7, 2-D plot for acceleration as frequency versus time

This harmonic wavelet analysis plot indicates that most of the harmonic wavelet energy of the response of the vehicle to the ride course is concentrated in the low-frequency area. With respect to the spring constants in the vehicle design, the natural frequency of the test vehicle frame is expected to be less that 5HZ. This natural frequency can be determined experimentally using a drop test and measuring the time-decay constant of the plot of how the springing motion damps. These plots suggest that it is possible to characterize the vehicle's response to the course using a few low-order wavelet coefficients. To do this, it is necessary to use a frequency ordered wavelet decomposition tree of the signal.

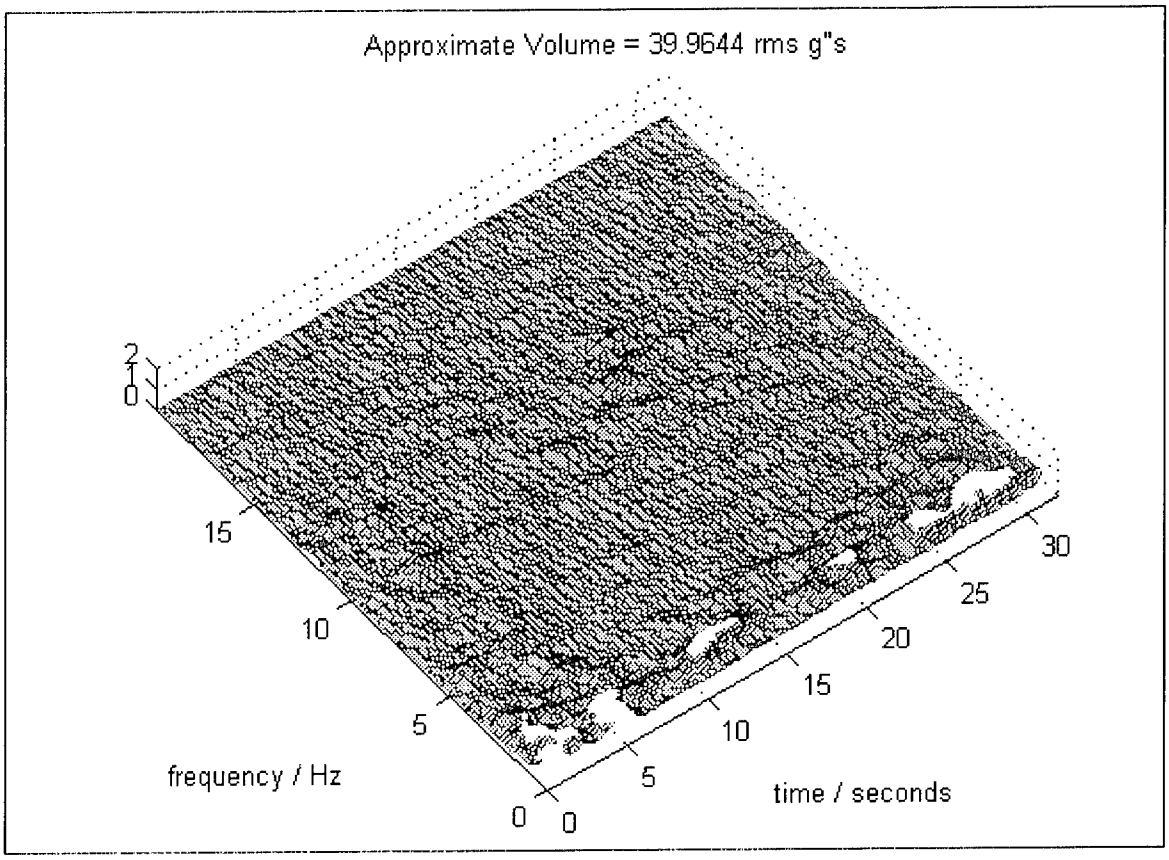

Figure 14. Channel 7, 3-D plot for acceleration as frequency versus time

Figure 15 shows the Meyer wavelet decomposition tree and frequency ordered wavelet coefficient values for the first 500 data points of the Letourneau Ride Course 1 data. The x-axis of the box (Figure 15, in box at lower right) is time and the y-axis is frequency. The wavelet decomposition tree has been cut off at the second level of decomposition. The number of boxes on the vertical y-axis corresponds to the number of frequency decomposition nodes on the lowest level in the wavelet decomposition tree. The results show that most of the wavelet energy is concentrated in the first node of the wavelet packet decomposition tree.

The analysis indicates that this test vehicle's vibrational response to the ride course can be characterized by the value of one Meyer wavelet coefficient.

Figure 16 shows the automatic de-noising of the Letourneau ride course ride meter data using a data compression method called soft wavelet thresholding. The graph in upper right box (Figure 16) in the yellow color is the reconstructed de-noised signal. The de-noising threshold applied was applied to cutoff wavelet coefficients whose sorted absolute value was below 0.77 of the maximum coefficient. This threshold was computed from a formula given in the book by Misiti et al. (1999) which involved a logarithm of the number of data points. As mentioned above, in this case, most of the wavelet packet energy is concentrated in the first node of the wavelet packet decomposition tree. Thus, thresholding

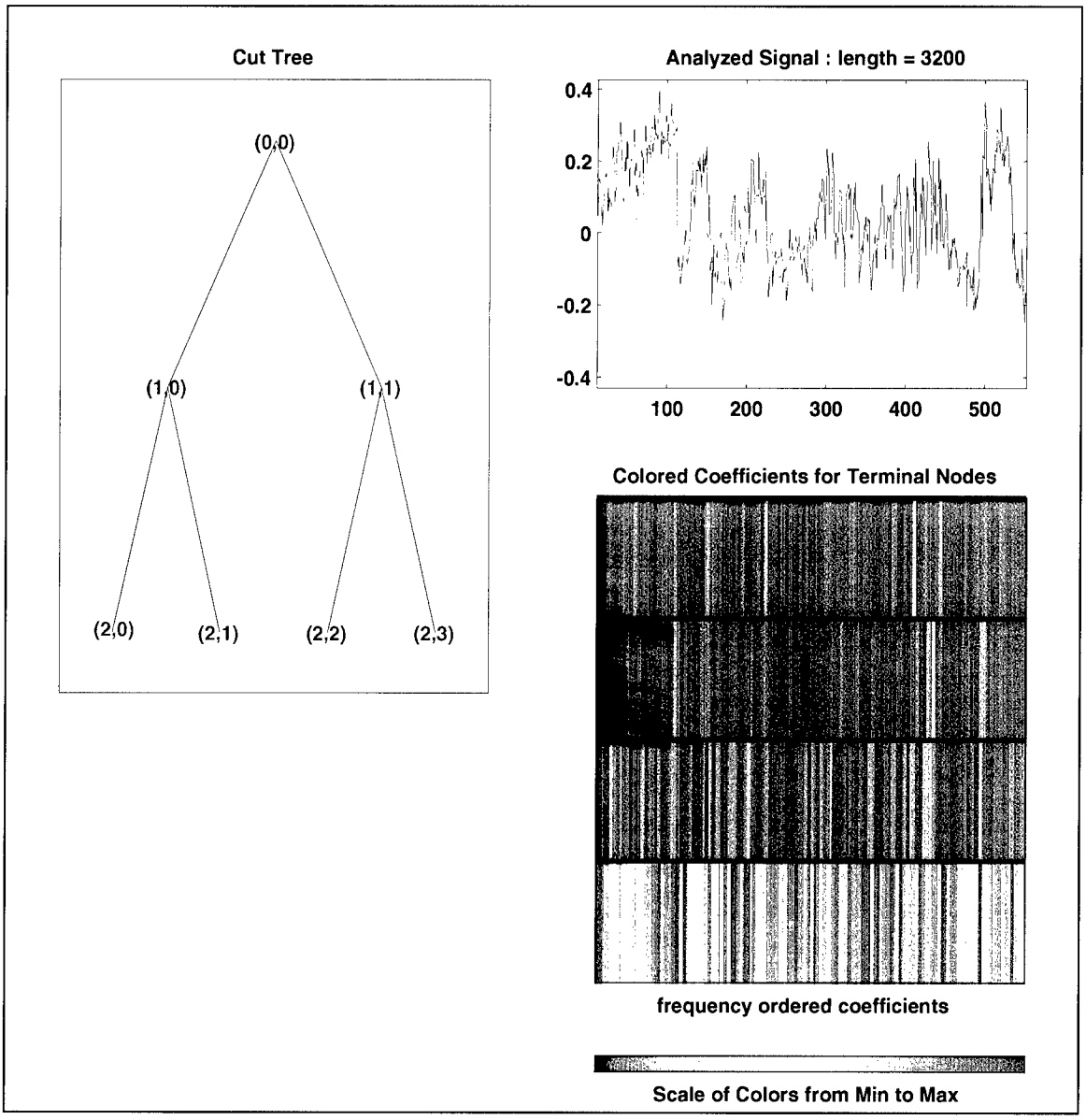

Figure 15. Meyer Wavelet Decomposition Tree

seems appropriate here. The x-axis of the box (Figure 16, box at lower right) is time and the y-axis is frequency. Higher-order frequency components have been dropped from the signal.

For each of the 3-D plots, such as Figure 6 or 8, it is possible to calculate the value of the area under the plotted surface. This value is in G's. The amplitude, or values plotted against the z-axis, is also in G's. The surface is actually a function called $A(t, f)$ where A is the amplitude of acceleration, t is time, and f is frequency. Integrating acceleration with respect to time yields velocity. Integrating $A(t, f)$, with respect to time and frequency, yields the original unit, because the units of frequency are $Hz = 1/t$.

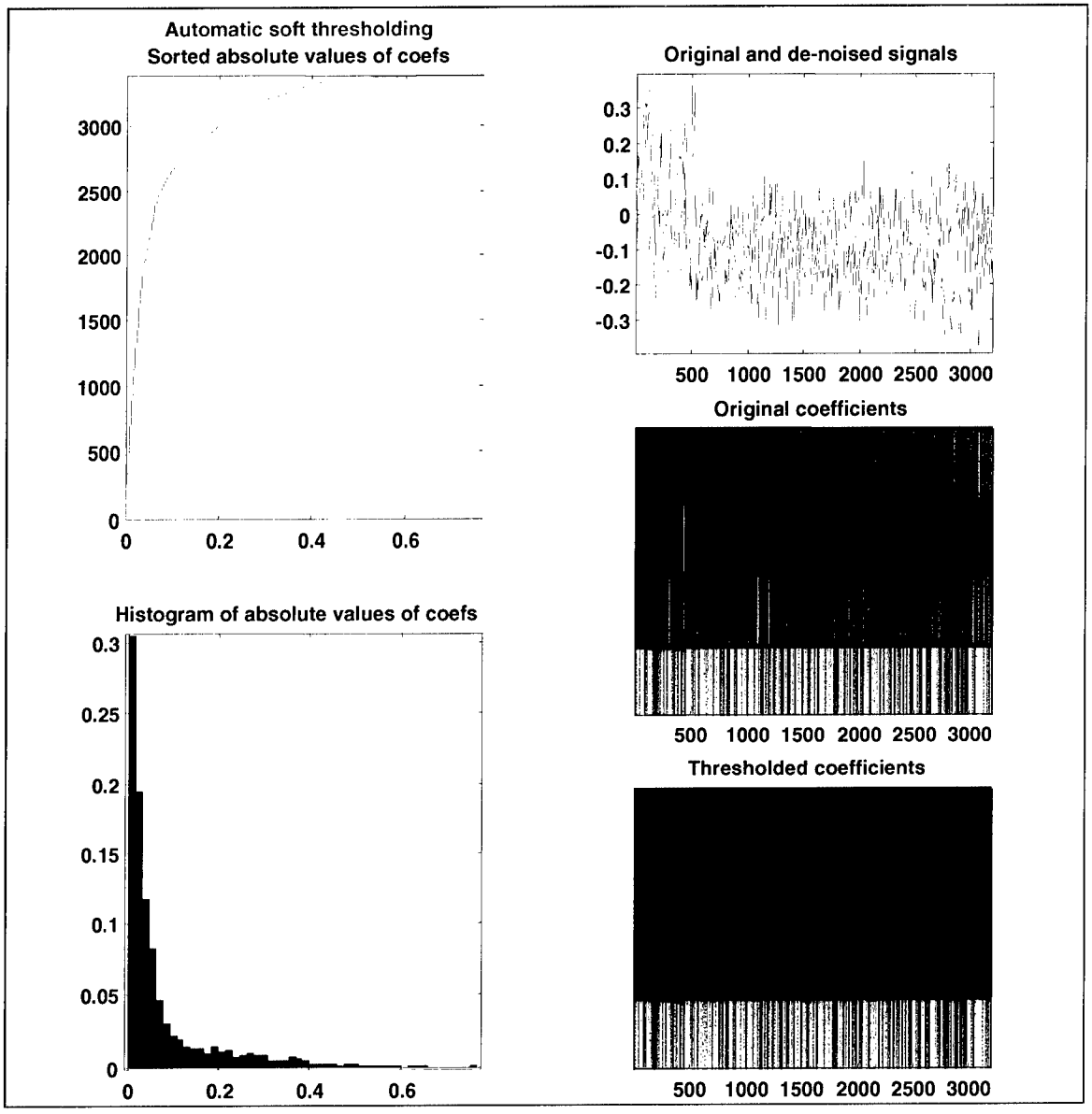

Figure 16. Ride course threshold coefficients

$$V = \iint A(t,f)dtdf = V\ t\ 1/t \tag{10}$$

Using these numbers and two selected channels, specifically channels 3 and 5, some very interesting features appear. The total volume numbers from Courses 1, 4, and 3 (the gravel road) were calculated. The total volume decreased as speed increased. This is to be expected because the length of time through the test track decreases as speed increases. Dividing the total volume g's by the time in the track, or the length of the record, the g's were for the most part constant, regardless of speed. The actual tabulated data are given in Table 3, and the plots are shown in Figures 17 and 18.

Table 3
G/sec Calculation Table

Course 1	**Ch3**		**Ch5**				
Rms=0.77	**Rear Left Axle**		**Front Right Axle**		**Time**		
	Total g's	**Total g's**	**Total g's**	**Total g's**	**sec**		
Speed	N	S	N	S	N	S	
10 mph	212.13	205.96	162.52	165.59	32.00	29.50	
15 mph	155.42	172.04	120.12	128.48	19.50	22.00	
20 mph	111.81	130.34	91.22	101.33	15.00	16.50	
	g's/sec	g's/sec	g's/sec	g's/sec			
10 mph	6.63	6.98	5.08	5.61			
15 mph	7.97	7.82	6.16	5.84			
20 mph	7.45	7.90	6.08	6.14			
Avg	7.35	7.57	5.77	5.86			
Course 4	**Ch3**		**Ch5**				
Rms=1.16	**Rear Left Axle**		**Front Right Axle**		**Time**		
	Total g's	**Total g's**	**Total g's**	**Total g's**	**sec**		
Speed	N	S	N	S	N	S	
10 mph	320.18	261.26	269.36	209.45	46.50	41.50	
15 mph	208.30	238.38	156.35	177.38	20.50	21.00	
20 mph	528.35	550.25	454.02	494.60	60.50	45.00	
	g's/sec	g's/sec	g's/sec	g's/sec			
10 mph	6.89	6.30	5.79	5.05			
15 mph	10.16	11.35	7.63	8.45			
20 mph	8.73	12.23	7.50	10.99			
Avg	8.59	9.96	6.97	8.16			
Course 3	**Ch3**		**Ch5**				
Rms=0.5	**Rear Left Axle**		**Front Right Axle**				
	Total g's	**Total g's**	**Total g's**	**Total g's**	**Time**		
Speed	N	S	N	S	N	S	
20 mph	86.13	82.62	64.64	66.35	16.5	17.5	
g's/sec	5.22	4.72	3.92	3.79			
		Rear Left Axle		**Front Right Axle**			
	RMS	N	S	N	S	avg	avg
	0.00	0.00	0.00	0.00	0.00	0.00	0.00
	0.50	5.22	4.72	3.92	3.79	4.97	3.85
	0.77	7.35	7.57	5.77	5.86	7.46	5.82
	1.16	8.59	9.96	6.97	8.16	9.28	7.57

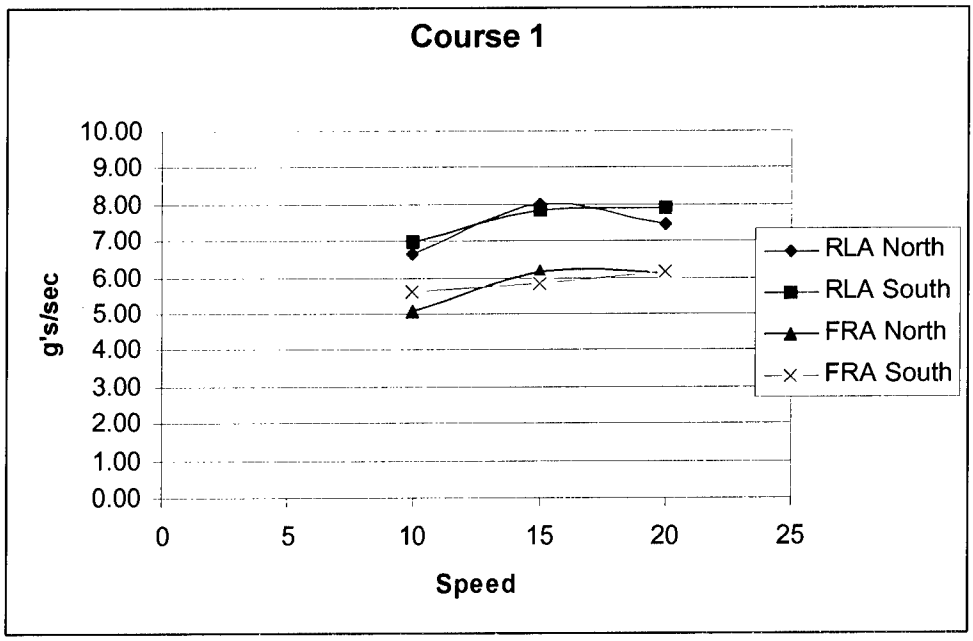

Figure 17. Plot for Course 1

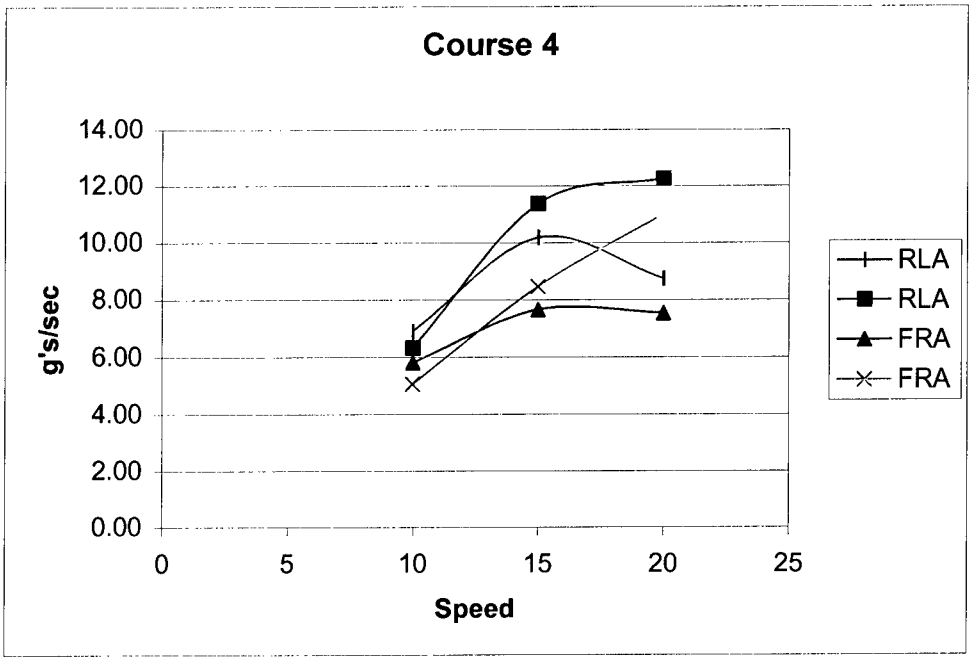

Figure 18. Plot for Course 4

The values of interest here are g's/sec. These values are plotted in the following figures: Figure 17, Course 1, in which the g's/sec are plotted as a function of speed, as well as for Figure 18, Course 4. The results for Course 1 show that the g's/sec are fairly constant with the differences being channel to channel. RLA is Right Left Axle and FRA is Front Right Axle. N and S are North and South. Course 1 appeared to be uniform regardless of which direction it was traversed. This did not appear to be the case with Course 4.

The reason Course 3 was included in this analysis, even though it presents only one point, was in order to use a lower rms value. Averaging the g's/sec values so that one value is representative for the speeds given in our test case yields the *Avg* values shown in Table 3. Taking these average values and presenting these values given in the lower portion of Table 3, plotting rms with respect to g's/sec results in Figure 19.

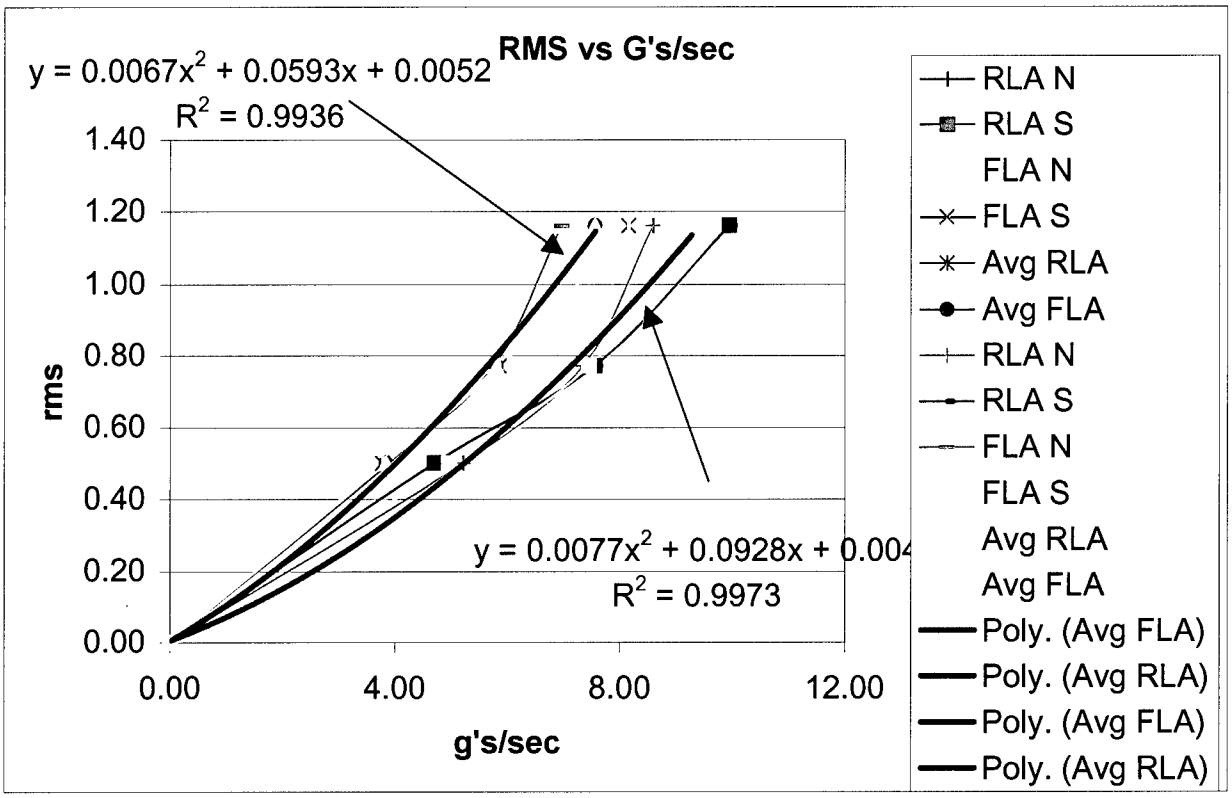

Figure 19. Relationship of total G volume and rms ride course values

This particular plot shows a second-order polynomial curve fit through the data. But keep in mind that it is only valid for limits of the data set presented. A broader scope could be obtained with different courses and at higher speeds with more experienced drivers.

$$rms = 0.0077(g's/\sec)^2 + 0.0928(g's/\sec) + 0.004 \quad (11)$$

For a single channel only.

Given a broad database of varying vehicles' ride performance data, one could make a sound judgment on the road condition's impact to that vehicle. The road could then be categorized and speed restrictions placed for that section of road. Figure 20 shows the absorbed power data collected from the ride meters as a function of rms, which is a family of curves for this vehicle. A 5-ton truck will obviously have a different family of curves, but the constant that remains is the indirectly measured rms value.

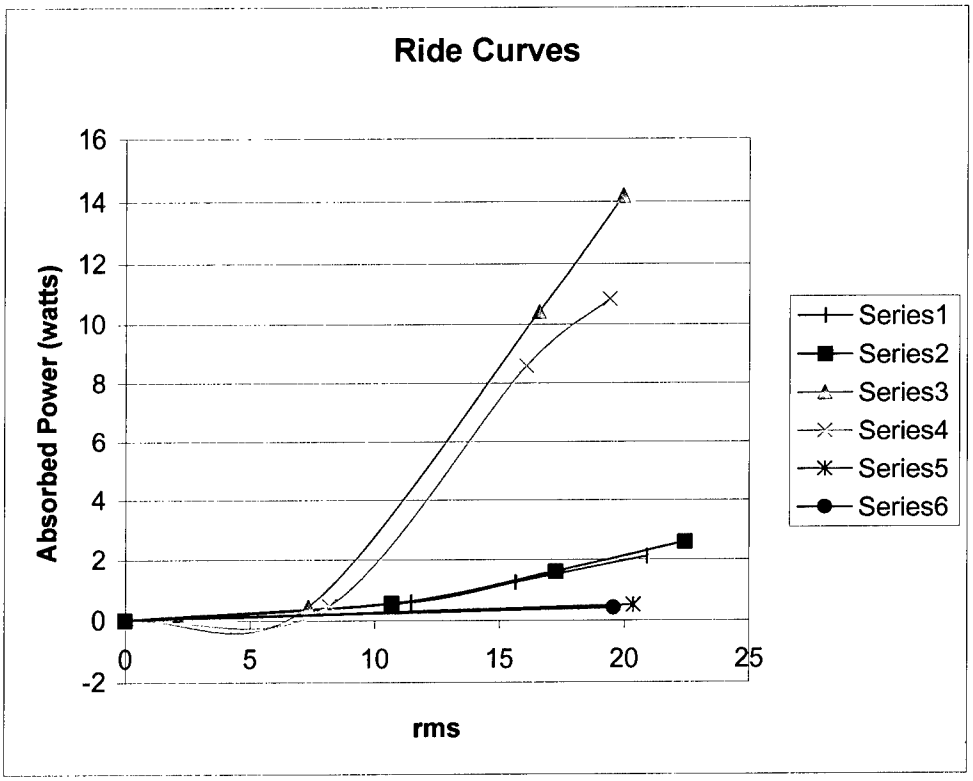

Figure 20. Absorbed power curves for Camouflage Tactical Utility Vehicle (CTUV) Suburban vehicle

5 Conclusions

A Meyer wavelet decomposition tree and frequency-ordered wavelet coefficient values were computed for the first 500 data points of the LeTourneau Ride Course 1 data. The wavelet decomposition tree was cut off at the second level of decomposition. The results showed that most of the wavelet energy is concentrated in the first node of the wavelet packet decomposition tree. Thus, the analysis indicates that for this ride course, this test vehicle's vibrational response to the ride course can be characterized by the value of one Meyer wavelet coefficient.

The first part of the LeTourneau Ride Course 1 was compared in terms of its Fourier power spectral transform and wavelet power spectral transform. The analysis indicated no need to use wavelet analysis to characterize the ride course itself. This result supports the conclusion that the root mean squared value distinguishing the course is adequate to characterize the course for experimental analysis of the vibrational response of the vehicle. The wavelet analysis did not show that significant parts of the frequency power spectrum of the course were left in the details of the first 3 levels of approximation to the signal. Thus, one would expect a Fourier transform or wavelet transform not to be affected by the response of the vehicle's vibrations to this part of the input. And, this supports the notion that for the off-road or cross-country ride courses the root mean square statistic is adequate to characterize the course for these experiments.

The harmonic wavelet analysis plot of the test vehicle's vibrational response to the LeTourneau Ride Course 1 indicates that most of the harmonic wavelet energy of the response of the vehicle to the ride course is concentrated in the low-frequency area. With respect to the spring constants in the vehicle design, the natural frequency of the test vehicle's frame is expected to be less that 5HZ. This natural frequency can be determined experimentally using a drop test and measuring the time decay constant of the plot of how the springing motion damps. These plots suggest that it is possible to characterize the vehicle's response to the course using few low-order wavelet coefficients. To do this, it is necessary to use a frequency-ordered wavelet decomposition tree of the signal.

The Mound Test Road results indicate that wavelets can be used to analyze the vehicle accelerometer data plotted with respect to time. A 3-D surface plot of the data can also be used as a measure of the total absorbed power by the vehicle over the ride course. This plot provides an alternate means of computing this other than using the ride meter, which has been in use for some years now. Finally, it

should be mentioned that road test tracks will not necessarily have simply designed power spectrums like the ERDC off-road courses. Thus, further research needs to be conducted to evaluate the usefulness of using wavelets to characterize road conditions.

References

Abry, P., Goncalves, P, and Flondrin, P. (1995). "Wavelets spectrum analysis and 1/f processes." *Wavelets and statistics.* Lecture Notes in Statistics No. 103, Springer Verlag, New York.

Chu, Charles K. (1992). *An introduction to wavelets.* Academic Press, Boston, MA.

_____. (1997). "Wavelets a mathematical tool of signal analysis," Society for Industrial and Applied Mathematics, Philadelphia, PA.

Daubechies, I. (1992). "Ten lectures on wavelets," Society for Industrial and Applied Mathematics, Philadelphia, PA.

Fourier J. (1955). *The analytical theory of heat.* Dover, New York.

Fournier, A. (1995). "Wavelets and their applications in computer graphics," SIGGRAPH 95 Course Notes, Association for Computing Machinery, NewYork.

Gabor, D. (1946). "Theory of Communication," *J.IEE* 93, 429-457.

Harrell, Andrew W. (1966). "Methodology for the curve fitting of non-linear ride curves." *Transactions of the Mathematics, Computer Science, Statistics Division of the Mississippi Academy of Science.* MAS Report 96-1, Jackson, MS.

_____. (1989). "Evaluating the effect of off-road obstacles on unit movement," Technical Report GL-89-4, U.S. Army Engineer Waterways Experiment Station, Vicksburg, MS.

Kay, Steven M. (1988). *Modern spectral estimation.* Prentice Hall, Englewood Cliffs, NJ.

Krantz, Stephen G. (1999). "A panorama of harmonic analysis." Mathematical Association of America. Washington DC.

Lewalle, J. (1995). "Tutorial on continuous wavelet analysis of experimental data." Syracuse University, New York.

Mallat, Stephane. (1998). *Wavelet tour of signal processing.* Academic Press, San Diego, CA.

Meyer and Ryan. (1993). *Wavelets, algorithms and applications.* Society for Industrial and Applied Mathematics, Philadelphia, PA.

Misiti, M., et al. (1996). *Wavelet toolbox.* The Math Works Inc., Natick MA.

Newland, D.E. (1993). *An introduction to random vibrations, spectral and wavelet analysis.* University of Cambridge, Longman, MA.

Newland, D., and Butler, G. (1999a). "Time varying cross-spectra for soil motion with damage." *17th ASME biennel conference on mechanical vibration and noise proceedings of the 1999 ASME Design Engineering Technical Conference.* Las Vegas, NV.

_____. (1999b). "Time frequency analysis of transient vibration data from earthquake centrifuge testing." *6th International Congress on Sound and Vibration.* Copenhagen.

Polikar, R. (1999). "The Wavelet Tutorial," Iowa State Computation Center, Ames, Iowa.

Press, William H., Teukolsky, Saul A., Flannery, Brian P., Vettering, William T., Misiti, Michel, Misiti, Yves, Oppenheim, Georges, and Poggi, Jean-Michael. (1992). "Numerical recipes in C." Cambridge University Press, New York.

Strichartz, R. S. (1993). "How to make wavelets," American Mathematical Monthly 100(6).

Torrence, C., and Compo, G. P. (1998). "A Practical guide to wavelets," *Bulletin of the American Meteorological Society* 79 (1).

Turnage, Gerald W., and Smith, Jerry L. (1983). "Adaptation and condensation of the Army mobility model for cross country mobility mapping," Technical Report GL-83-12, U.S. Army Engineer Waterways Experiment Station, Vicksburg, MS.

Ueda, M., and Lodha, S. (1995). *Wavelets, an elementary introduction and examples.* University of California, Santa Cruz.

Walker, James S. (1999). *Primer on wavelets and their scientific applications.* Chapman & Hall, CRC Press, Boca Raton, FL.

Yamada, M., and Sasaki, F. (1998). "Wavelet analysis of atmospheric wind turbulent fluid, and seismic acceleration data." *Wavelets and their applications.* Society for Industrial and Applied Mathematics, Philadelphia PA.

Internet Sites

Rice University: www.dsp.rice.edu.
ATT Research Labs: www.wavelet.org.
Stanford University: www.stat.standford.edu/~wavelab

Appendix A
Wavelet Analyses of the LeTourneau Ride Courses

The graphs, Figures A1 through A6, in this appendix show a Daubechies (1992)[1] wavelet analysis of the detrended ride course elevation density. The first 120 ft and 300 ft of the LeTourneau 1 Ride Course (data in Figure A1) were analyzed separately. Figure A2 shows the detrended values of the elevations in the same course. Figure A3 shows the power spectral density computed from the detrended elevations. Figure A4 shows a Daubechies multilevel decomposition using the second Daubechies wavelet family. Top left graph of Figure A4 is the level 3 approximation to the spectral density. The remaining graphs display the next three levels of detail in the wavelet analysis. The ratios of the magnitudes of the values on the y-axis of the details versus the approximation indicate that it is hard to characterize the ride course by this type of approximation.[2]

The term rms (root mean squared elevation, inches) is used by the Mobility Systems Branch, Geotechnical and Structures Laboratory (GSL), U.S. Army Engineer Research and Development Center (ERDC), Vicksburg, MS, site, in the characterization of the surface roughness of terrain. It is determined by first detrending (subtracting the linearly increasing or decreasing component) the surface elevation measurements taken at 1-ft intervals in the terrain profile and then computing the ordinary square root of the variances of the measurements from the detrended value. The paper by Harrell (1966) gives a fuller discussion of how rms is used in vehicle tests to determine ride-limiting speed. Ride-limiting speed represents the speed at which vehicle vibrations at the driver's seat reach absorbed power limits of 6 watts in the vertical direction.

Figure A3 depicts the power spectral density of the profile elevation in the first 120 ft of the LeTourneau Ride Course 1 (left track). The graphs plotted horizontally up to the limits of the nyquist sampling frequency (50 cycles/second) of the instrumentation on the test vehicle. The values were calculated by taking discrete Fourier transforms of the data.

[1] References are listed at the end of the main text of this report.

[2] Methodology for the wavelet approximations is that in the MATLAB toolbox book by Misiti et al (1996).

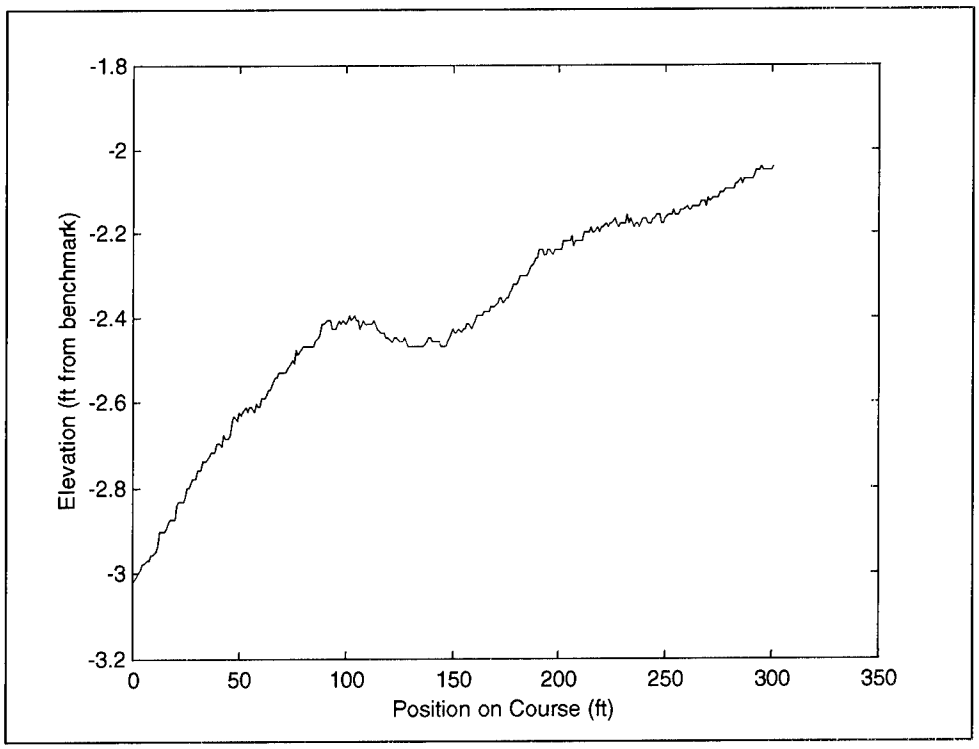

Figure A1. Elevation profile of LeTourneau Ride Course

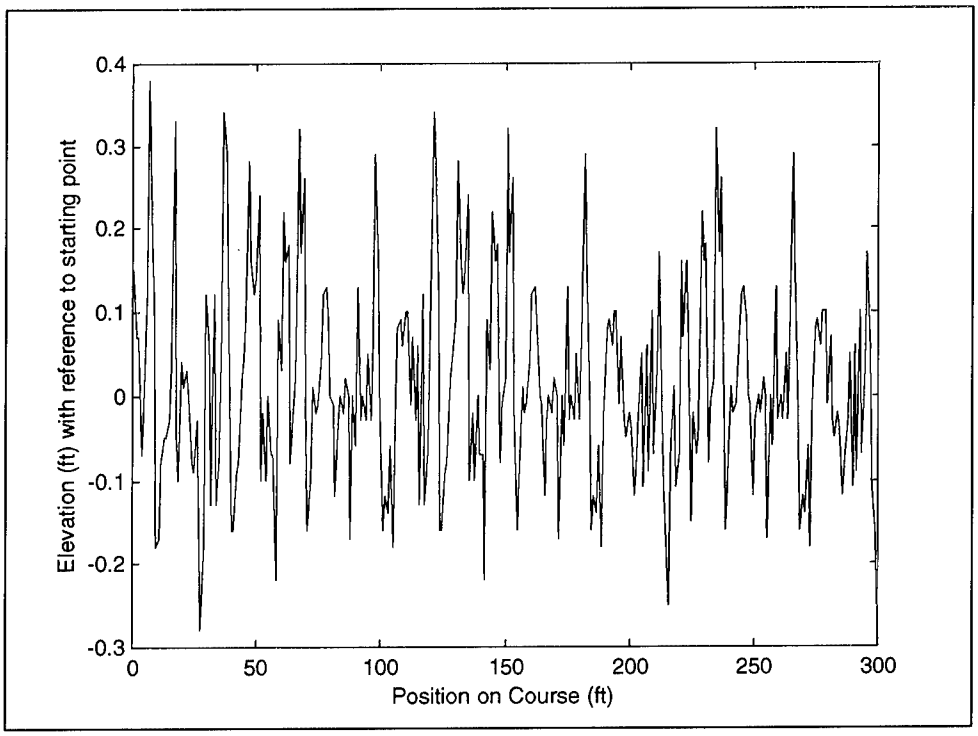

Figure A2. Detrended elevation profile

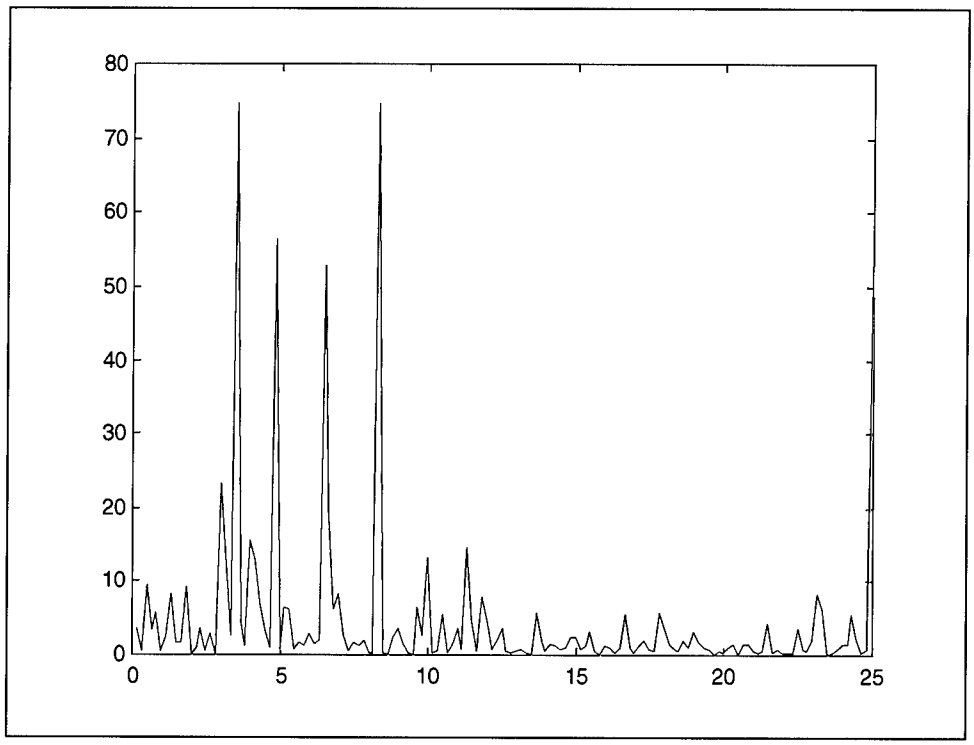

Figure A3. Power spectral density of the ride course elevation profile, LeTourneau 1 (left track)

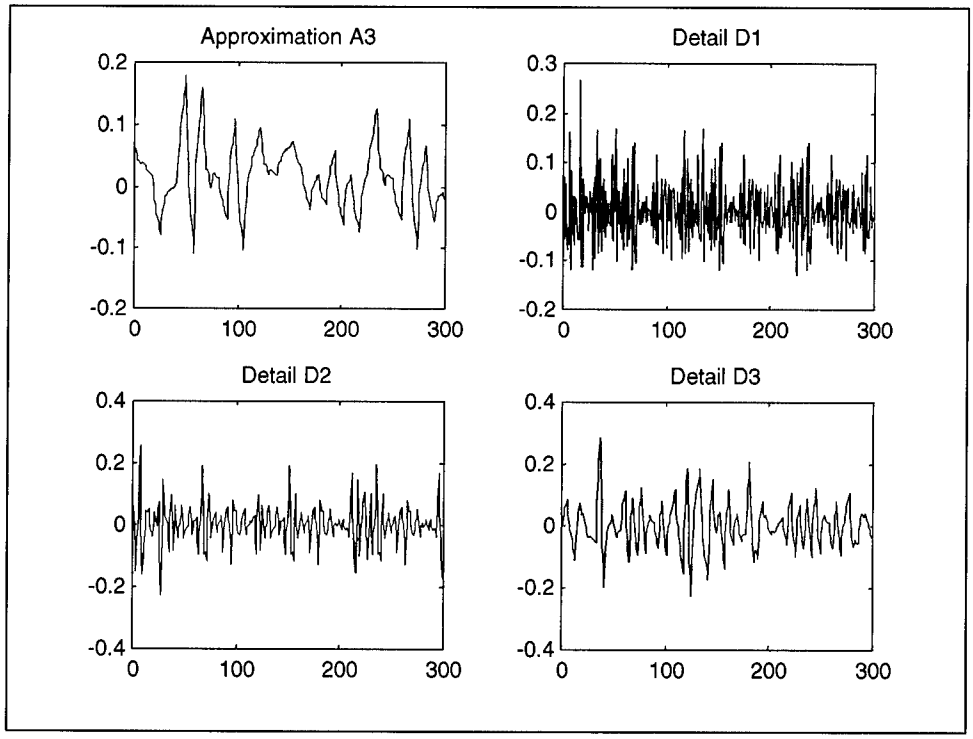

Figure A4. Wavelet analysis of ride course 1 (0 to 120 ft)

Wavelet Approximation of Detrended Ride Course Elevations

The graphs shown in Figure A4 and A5 show a Daubechies (1992) wavelet analysis of the detrended ride course elevation density. Again, the first 120 ft of the LeTourneau Ride Course 1 (Figure A4) and the entire 300 feet (Figure A5) were analyzed. A Daubechies multilevel decomposition was accomplished using the second Daubechies wavelet family. The top left graph is the level 3 approximation to the spectral density. The remaining graphs display the next three levels of detail in the wavelet analysis (D1, D2, and D3). The ratios of the magnitudes of the values on the y-axis of the details versus the approximation indicate that it is difficult to characterize the ride course using detrended elevations with this type of approximation.[1]

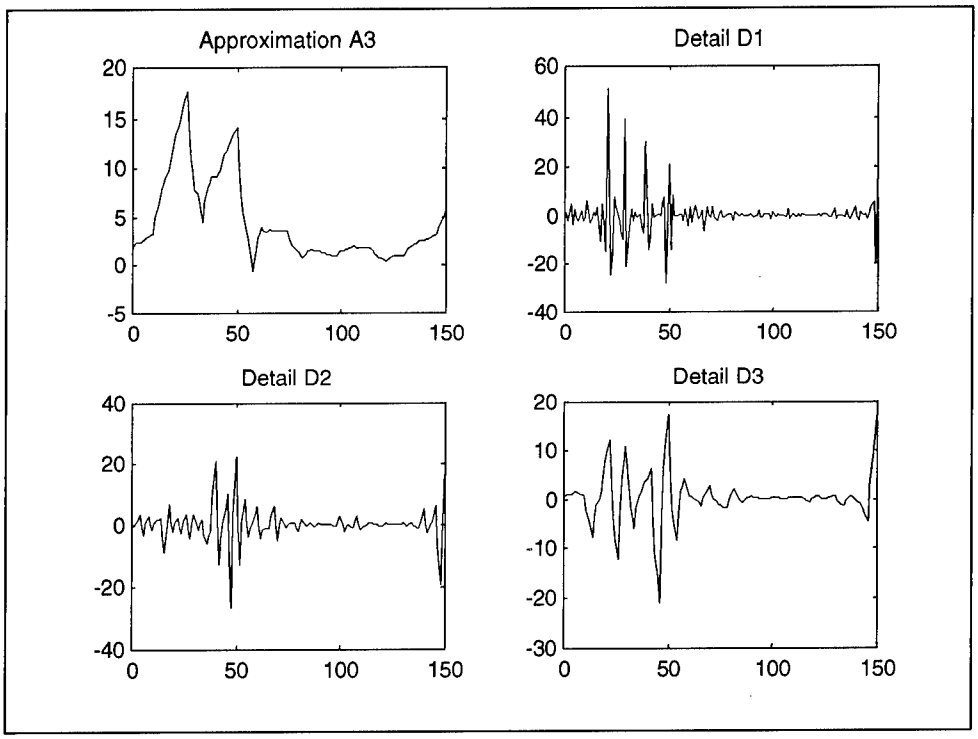

Figure A5. Wavelet analysis of ride course 1 (0 to 300 ft)

[1] Methodology for the wavelet approximations is that in the MATLAB toolbox book by Misti et al. (1996), listed in references following main text.

Wavelet Approximation of Ride Course Power Spectral Density Curve

Figure A6 shows the same analysis as the previous figures except, in this case, the same wavelet families were used to approximate the power spectral density graphs.

Here again, comparing the magnitude of the detail coefficients to the level 3 approximation coefficients, the approximation does not adequately capture the data to the detail desired.

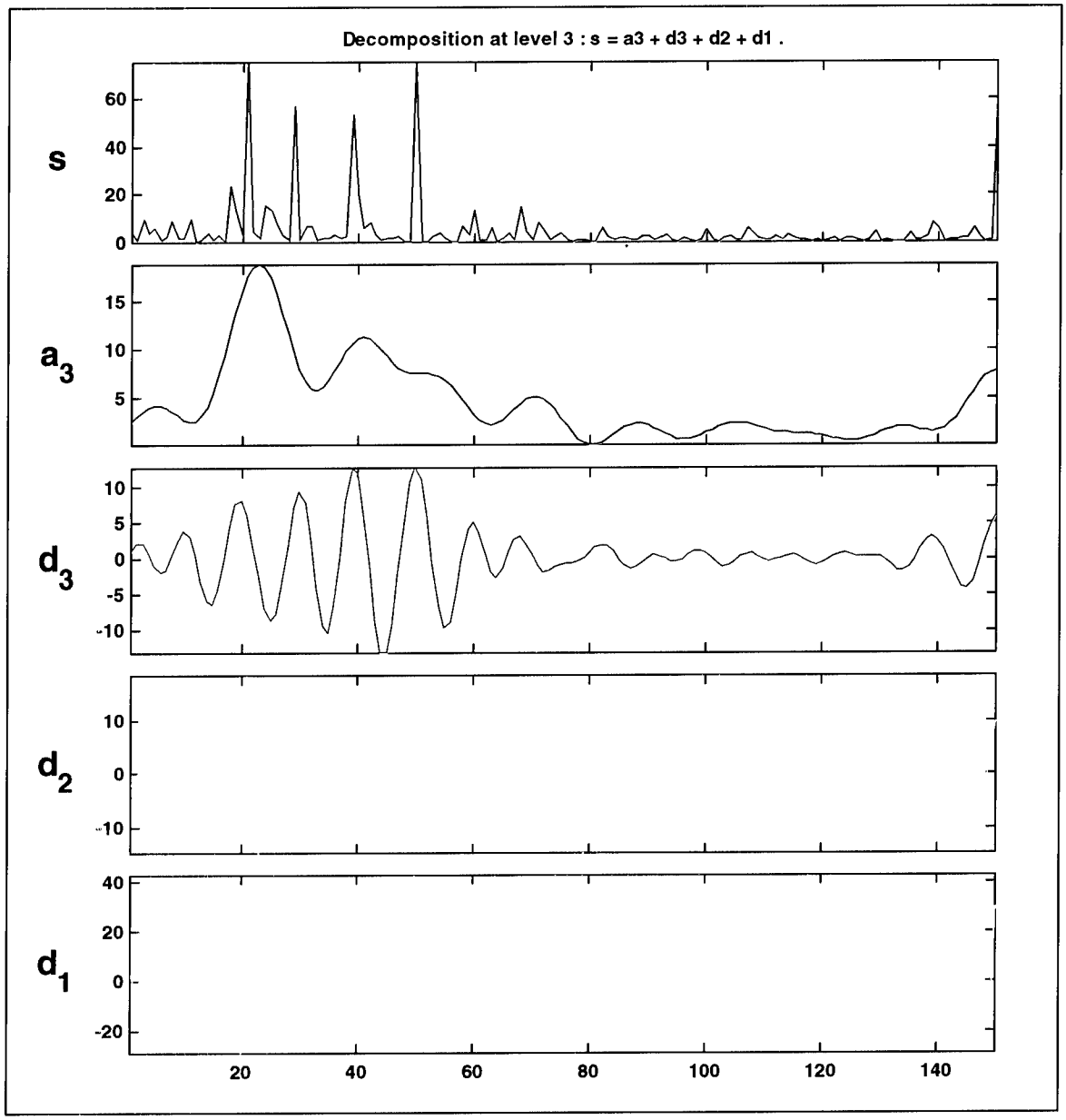

Figure A6. Wavelet analysis of ride course elevation profile power spectral density

Appendix B
Index

REPORT DOCUMENTATION PAGE

Form Approved
OMB No. 0704-0188

1. REPORT DATE *(DD-MM-YYYY)*	2. REPORT TYPE	3. DATES COVERED *(From - To)*
August 2001	Final report	

4. TITLE AND SUBTITLE
Application of Wavelet Analysis to Logistics Test Vehicle Ride Experiment Results

5a. CONTRACT NUMBER

5b. GRANT NUMBER

5c. PROGRAM ELEMENT NUMBER

6. AUTHOR(S)
Andrew W. Harrell, Cliff Grey, William Willoughby

5d. PROJECT NUMBER

5e. TASK NUMBER

5f. WORK UNIT NUMBER

7. PERFORMING ORGANIZATION NAME(S) AND ADDRESS(ES)

U.S. Army Engineer Research and Development Center
Geotechnical and Structures Laboratory
3909 Halls Ferry Road
Vicksburg, MS 39180-6199

8. PERFORMING ORGANIZATION REPORT NUMBER

ERDC/GSL TR-01-16

9. SPONSORING / MONITORING AGENCY NAME(S) AND ADDRESS(ES)
U.S. Army Corps of Engineers
Washington, DC 20314-1000

10. SPONSOR/MONITOR'S ACRONYM(S)

11. SPONSOR/MONITOR'S REPORT NUMBER(S)

12. DISTRIBUTION / AVAILABILITY STATEMENT
Approved for public release; distribution is unlimited.

13. SUPPLEMENTARY NOTES

14. ABSTRACT

The purpose of this study was to develop and recommend a methodology for evaluating tactical support road situations which will assist in determining appropriate convoy speeds, evaluate the use of bypass routes around lost critical nodes in the infrastructure, and allow the computation of road capacities for determining the logistic vehicle requirements for various tactical scenarios. In this report, an innovative methodology using wavelet transforms is developed. These are used to characterize the vehicle's vibrational response to ride conditions while traversing nondeformable areas of known surface roughness. Because the mathematical background necessary to understand the application of wavelets to vehicle vibrational response is relatively new, a short review of wavelet mathematics is also included in this report. The development of wavelet technology as an alternative means to characterize the surface roughness of the ride courses through use of the LSV in a similar manner is also described.

15. SUBJECT TERMS
Lines of communication; NATO Reference Mobility Model (NRMM); Ride tests; Wavelet analysis; Logistic test vehicle; Repair of roadways; Vibration analysis

16. SECURITY CLASSIFICATION OF:			17. LIMITATION OF ABSTRACT	18. NUMBER OF PAGES	19a. NAME OF RESPONSIBLE PERSON
a. REPORT	b. ABSTRACT	c. THIS PAGE			19b. TELEPHONE NUMBER *(include area code)*
UNCLASSIFIED	UNCLASSIFIED	UNCLASSIFIED		47	

Destroy this report when no longer needed. Do not return it to the originator.